[American Journal of Science, Vol. 301, April/May, 2001, P. 455–485]

# UPLIFT, SHORTENING, AND STEADY STATE TOPOGRAPHY IN ACTIVE MOUNTAIN BELTS

SEAN D. WILLETT*, RUDY SLINGERLAND**, and NIELS HOVIUS***

**ABSTRACT. We present a tectonic, surface process model used to investigate the role of horizontal shortening in convergent orogens and the effects on steady-state topography. The tectonic model consists of a specified velocity field for the Earth's surface and includes a constant uplift rate and a constant horizontal strain rate which varies to reflect the relative importance of frontal accretion and underplating in an orogenic wedge. The surface process model includes incision of a network of rivers formed by collection of applied precipitation and diffusive hillslope mass transfer. Three non-dimensional parameters describe this model: a ratio of the maximum horizontal velocity to the vertical velocity, a Peclet number expressing the efficiency of the hillslope diffusion relative to the uplift rate, and a fluvial "erosion number" reflecting the fluvial incision efficiency relative to the uplift rate. A series of models are presented demonstrating the resultant steady-state landforms parameterized by these three numbers. A finite velocity ratio results in an asymmetric form to the model mountain range, although the magnitude of the asymmetry also depends on the Peclet number. Topographic steady-state is achieved faster for models with no horizontal component to the velocity field. With finite horizontal velocity, topographic steady state is achieved only at the scale of the entire mountain range; even the first order drainage basins are unstable with time in the presence of horizontal shortening. We compare our model results to topographic profiles from active mountain ranges in Taiwan, New Zealand, and the Olympic Mountains of Washington state. All these examples exhibit asymmetric topographic form with the asymmetry consistent with the polarity of subduction, suggesting that horizontal tectonic motion is affecting the macro-geomorphic form of these ranges.**

## INTRODUCTION

The strong feedbacks between the tectonic processes that create topography and the erosion processes that destroy topography are most evident in active, compressional mountain belts. At convergent plate boundaries, crustal contraction may lead to high rates of surface uplift as tectonically thickened crust is isostatically compensated. These high uplift rates and excess topography lead to high erosion rates through the increase in relief (Ahnert, 1970) and climatic factors such as an orographic increase in precipitation (Beaumont, Fullsack, and Hamilton, 1992; Willett, 1999). This increase in erosion rate tends to decrease excess elevation, thereby leading to a damped dynamic system in which the tectonic uplift and erosion drive the excess elevation toward a stable or steady state. A topographic steady state is most likely to be achieved in small, convergent mountain belts with high rates of erosion and moderate rates of crustal accretion and surface uplift. Such conditions have been hypothesized to exist in New Zealand (Adams, 1980; Kamp, Green, and White, 1989; Norris, Koons, and Cooper, 1990; Hovius, Stark, and Allen, 1997), Taiwan (Li, 1976; Suppe, 1981; Hovius and others, 2000) and the Olympic Mountains segment of the Cascadia forearc (Brandon, Roden-Tice, and Garver, 1998).

It is important to note that the balance between tectonic and erosion processes is not as simple as an equating of surface uplift rates and erosion rates on a pointwise basis. At steady state, erosion must be in balance with the full tectonic velocity field. This field has both vertical and horizontal components. Horizontal displacements or

* Department of Earth and Space Sciences, University of Washington, Seattle, Washington 98195
** Department of Geosciences, The Pennsylvania State University, University Park, Pennsylvania 16802
*** Department of Earth Sciences, Cambridge University,Cambridge, CB2 3EQ United Kingdom

velocities are significant in essentially all tectonic settings including convergent mountain belts. In fact, they are typically larger than the vertical component by about an order of magnitude. This point has not been fully appreciated in the past, and it is common to see topographic steady state defined in the literature as the condition that uplift rate is equal to erosion rate.

Here we investigate topographic response to crustal thickening and mountain building using a tectonic kinematic model, which includes both vertical and horizontal surface velocities. We have coupled the tectonic model to a surface process model (SPM) to create orogenic wedge models appropriate for subduction plate boundaries and small collisional orogens (Davis, Suppe, and Dahlen, 1983; Platt, 1986; Willett, Beaumont, and Fullsack, 1993) and to explore the importance of horizontal shortening to the large-scale morphology of such orogens. Our results demonstrate that horizontal advection plays an important role in determining the macrogeomorphology of mountain belts and may be the principal cause of topographic asymmetry and the curious drainage patterns seen in selected orogens.

## TECTONIC, SURFACE PROCESS MODEL

A number of planform, surface process models have been developed in recent years, specifically to investigate the response of topography to tectonic forcing (Beaumont, Kooi, and Willett, 2000), but in most cases the investigators have limited their studies to a simple vertical uplift pattern. Studies that have considered horizontal motions have generally been in extensional (Densmore, Anderson, and Ellis, 1998) or strike-slip tectonic regimes (Anderson, 1990), although the study of Beaumont, Fullsack, and Hamilton (1992) included the horizontal displacements predicted from a finite element model. Surface process models have been applied at a variety of scales from single catchments (Willgoose, Bras, and Rodriguea-Iturbe, 1991; Tucker and Slingerland, 1997) to full orogenic belts (Beaumont, Fullsack, and Hamilton, 1992). Kooi and Beaumont (1996), for instance, investigated the topographic response to regional uplift, simulating a crustal-scale orogenic process. Their focus was primarily on the timescales of the landscape response as measured by topography and sediment fluxes from the orogenic system. For a constant uplift rate, they found that steady-state topography was reached in a time that scaled with the uplift rate, width of the mountain belt, and physical parameters of the erosion model.

The model used here contains independent components for the tectonics and surface processes. The tectonic model is purely kinematic without feedback; it consists of a fully specified velocity field in two-dimensions and is independent of erosion rate or total erosion. The tectonic model produces excess topography that serves as the source term for the surface process model (SPM), which is physically based as described below.

### *Tectonic Model*

The tectonic model is designed to represent the crustal kinematics associated with subduction at a convergent orogen. At oceanic plate subduction boundaries, orogenesis and mountain-building occur in response to off-scraping of marine sediments, leading to the formation of an accretionary wedge. If an accretionary wedge grows large enough to emerge above sealevel, it can form a significant mountain range. Examples of such ranges include the Coast Ranges, Olympics and Insular ranges of the Cascadia margin (Tabor and Cady, 1978), and the Kenai Peninsula of Alaska. In intracontinental settings, convergent orogenesis is also associated with deep subduction. In orogens small enough to be imaged by seismic reflection techniques, it has been proposed that contraction of the mantle and crust is achieved by subduction of one plate. Examples of this process include the European Alps (Pfiffner, 1992; Schmid and others, 1996), the Pyrenees (Munoz, 1992), the Southern Alps of New Zealand

(Walcott, 1998) and Taiwan (Suppe, 1981; Davis, Suppe, and Dahlen, 1983). This kinematic model has important implications for the surface patterns of horizontal motion and uplift velocity. In a subduction-accretion system, all crustal mass delivered into an orogen is derived from one plate. There is thus a polarity associated with the process so that all material is moving toward the over-riding plate. There is also an upward component of motion associated with crustal thickening and the resultant isostatic surface uplift.

Alternative models for orogenesis have been proposed, the most common of which proposes that convergence is resolved by pure-shear shortening of the entire continental lithosphere (England and McKenzie, 1982). This model may be applicable to large continental-scale orogens, but it is almost certainly not applicable to oceanic subduction orogens. Molnar and others (1999) recently suggested that pure-shear shortening was appropriate for the Southern Alps of New Zealand based on teleseismic delay times. However, the inability of this model to explain the asymmetry in exhumation patterns (Norris, Koons, and Cooper, 1991; Walcott, 1998) and topography as discussed here suggests that its applicability to small orogens such as Taiwan or the Southern Alps of New Zealand remains unlikely other than perhaps in some mixed form of detachment and pure-shear shortening (Pysklywec, Beaumont, and Fullack, 2000).

The subduction-accretion process leads to the formation of an orogenic wedge with a geometry dictated by the mechanical properties of the crustal material in its interior. In particular, critical wedge theory (Davis, Suppe, and Dahlen, 1983) predicts that an orogenic wedge will attain a critical surface slope maintained by continued accretion. The rear of this accretionary wedge is defined by a mechanical "backstop" over which accreted crustal material is backthrust, forming a wedge tapering in the opposite direction (fig. 1) (Willett, Beaumont, and Fullsack, 1993). The large-scale morphology of a mountain range formed in this manner is thus characterized by back-to-back wedges that taper in opposite directions with a topographic crest between the two. Deformational structures also typically verge in opposite directions in response to the surface topographic slope. The polarity of the accretion process implicit in this tectonic model is specified by referring to the accreting side of the orogen as the prowedge and the opposite, non-accreting side as the retrowedge (fig. 1), and we will use this terminology throughout this paper.

The precise spatial patterns of horizontal and vertical rock velocity are a function of where material is accreted and how it deforms within the accretionary wedge. We can distinguish between two endmember modes of crustal accretion, as illustrated in figure 1. In the first case, material is assumed to be dominantly accreted at or near the toe of the crustal orogen, typically as thrust slices in the frontal regions of an accretionary wedge or fold-and-thrust belt (fig. 1A). If all crustal material in an orogen is added by frontal accretion, the orogenic wedge is required to deform internally so that material can be supplied to the rearward regions of the wedge in order to maintain the self-similar growth and wedge geometry implied by critical wedge theory. Although there are many strain fields that can accomplish this, the simplest involves vertical extension and horizontal shortening of a column of rock (fig. 1A). The resultant velocity field would thus have a vertical component and a horizontal component that decrease toward the rear of the orogenic wedge. Ignoring the time-dependent increase in toe-to-backstop length of the orogenic wedge, the surface velocity field consistent with self-similar growth will have a constant vertical component and a horizontal component that decreases linearly from the toe to the rear of the wedge. This velocity field is also consistent with topographic steady state such that the cross-sectional form of the orogen in figure 1A does not change with time. This velocity field in the coordinate system of figure 1A is thus:

$$u = U,$$

$$v = \frac{V_c}{L} x \tag{1}$$

where $u$ and $v$ are the vertical and horizontal surface velocities, respectively, $U$ is the scalar magnitude of the surface uplift rate, and $V_c$ is the convergence velocity. The

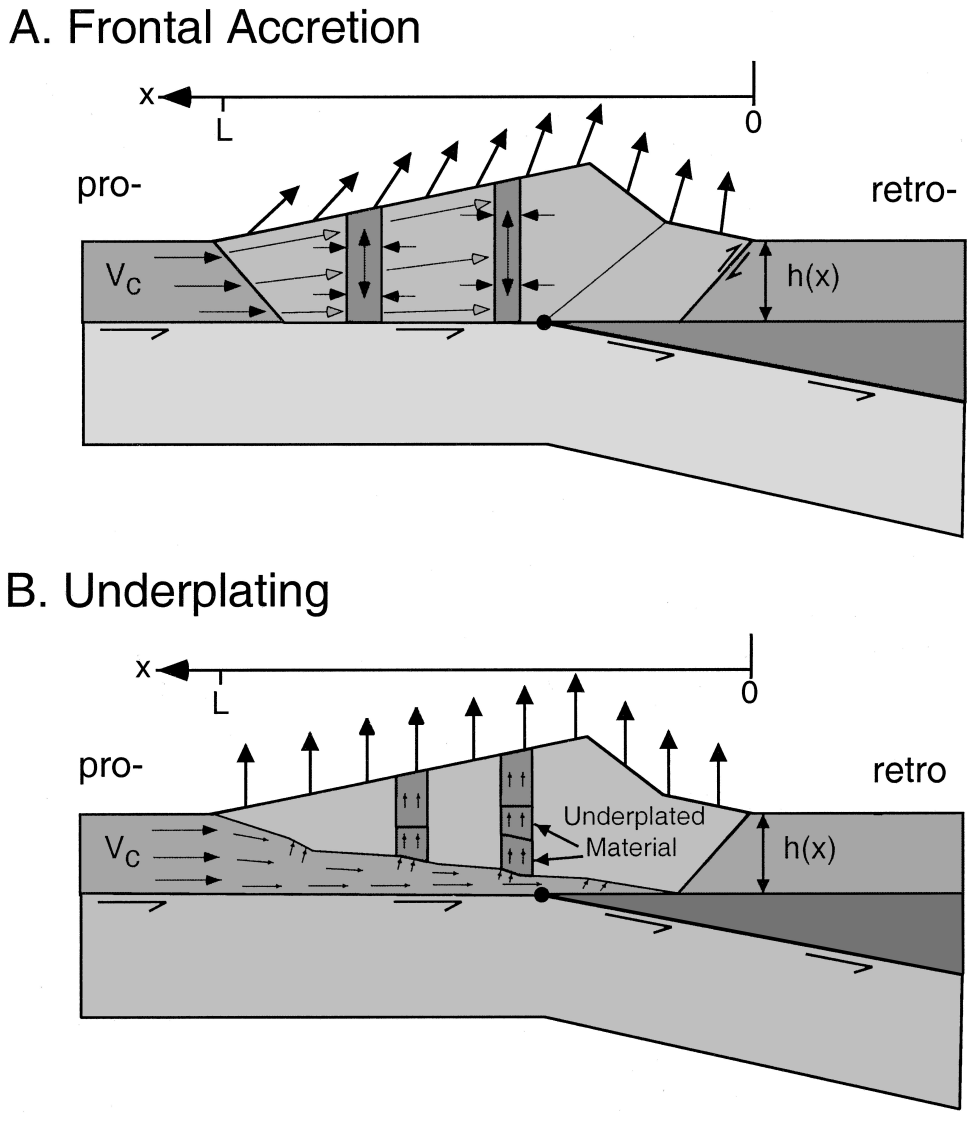


Fig. 1. Modes of orogenic wedge growth used as tectonic model in this paper. (A) Orogenic wedge grows by mass added through frontal accretion process. Wedge deforms by pure shear such that a vertical column extends vertically and shortens horizontally. Vertical component of surface velocity is constant. Horizontal component of surface velocity increases linearly in $x$ from 0 to $L$ reaching a maximum value of $V_c$, the convergence velocity. (B) Orogenic growth by underplating. Wedge does not shorten horizontally and thus has no horizontal velocity. Columns of rock move vertically at a constant rate in response to addition of new material at base of the wedge.

linear increase in horizontal velocity implies a constant horizontal strain rate, since longitudinal strain rate in $x$ is $dv/dx$. At steady state, for accretion of a constant thickness of new material, $h$, conservation of mass requires that $U = V_c h/L$.

The alternative mechanism for crustal accretion is by deep underplating by which material underthrusts the orogenic wedge to significant depths where it is subsequently accreted to the base of the wedge (fig. 1B). This process is consistent with stepping-down of the level of a decollement beneath accretionary wedges and the formation of crustal duplexes with roof and basal thrusts. In principle, crustal material can be added anywhere along the base of the orogenic wedge. If material is added uniformly along the base, the overlying wedge would be uplifted uniformly, maintaining the condition of self-similar growth or constant cross-sectional form if erosion is maintaining a steady state. This is achieved with little or no internal strain, so that the resultant velocity field is quite different from that of figure 1A. In fact, the horizontal component of the surface velocity could potentially be zero, so the surface velocity is specified entirely by the vertical component: $u = U$.

The addition of crustal material to an orogenic wedge from the subducting plate can occur by either frontal accretion or underplating or both. In active systems, the horizontal strain rate reflects the relative importance of frontal accretion. The zero strain rate endmember corresponds to the case of no frontal accretion.

This kinematic model involves several simplifications with respect to actual orogenic systems. The assumption of spatially constant uplift rate and horizontal velocity neglects variations associated with specific structures such as individual thrust sheets which can exhibit differential motion over a timescale of 100kyr. Such differential uplift can affect range morphology as in the fold-and-thrust belt of western Taiwan where large longitudinal river valleys, trending nearly parallel to the range are associated with individual thrust structures. A similar pattern is observed on the east side of the Southern Alps of New Zealand with the added complexity of distributed dextral shear leading to an oblique drainage pattern (Koons, 1995). Our assumption of constant uplift rate does not permit the development of such longitudinal rivers, thereby emphasizing transverse river drainages.

The validity of a spatially-constant uplift rate as an appropriate average over geologic time is difficult to assess, and this is a difficult quantity to measure. England and Molnar (1990) pointed out some of the difficulties and mistaken interpretations of the various observations used to determine the rate of rock uplift at the Earth's surface. In fact, the problem is even more complex than they suggest, if one also considers the effects of horizontal motion of the surface and subsurface rocks. In this case, measurements of exhumation, as provided by thermochronometers or metamorphic grade, cannot be used to infer rock uplift rates at a specific point as it reflects the uplift rate averaged over the entire kinematic path taken by an exhumed rock. For example, the strong gradient in total exhumation exhibited with distance east of the Alpine Fault in the Southern Alps of New Zealand is frequently cited as evidence for differential rock uplift rates with the highest rates adjacent to the fault (Wellman, 1979; Tippet and Kamp, 1993; Koons, 1995). However, this pattern could simply reflect the different paths taken by rocks presently at the surface with the higher degree of exhumation reflecting a deeper particle path (fig. 1), with surface uplift rates spatially constant. Geomorphic estimates of rock uplift are typically based on markers such as fluvial terraces, which provide estimates of incision, but not necessarily rock uplift rate (Pazzaglia and Brandon, 2001), making these data problematic as well. Geodetic data can be used to constrain surface uplift but only over a short timescale, so that displacements associated with the earthquake cycle on specific faults often dominate. Given these problems, we find little evidence strongly supporting uplift patterns

systematically different from a constant rate of uplift and therefore use a constant rate to simplify the subsequent analysis.

The remaining assumption that the horizontal displacement goes linearly to zero at the retro-deformation front is also a simplification of our kinematic model. This neglects the horizontal component of displacement on the bounding structure, although the vertical component is still included. Since the horizontal velocity of material just across the deformation front is zero by definition, the question reduces to how much of the total convergence is accommodated on this bounding structure. This seems to vary considerably from orogen to orogen. In the Southern Alps, nearly half the convergence seems to be accommodated on or near the Alpine fault (Beavan and others, 1999). In Taiwan, the comparable structure juxtaposes greenschist facies metasediments of the Central Range and Quaternary sediments of the Longitudinal Valley. This fault has not been described in outcrop and in places is stitched by undeformed fluvial terraces suggesting that it is only intermittently active or has very low displacement rates (Willemin and Kneupfer, 1994), so that shortening is distributed on other structures through the orogen. Thus although it might be appropriate to include a step in the horizontal velocity at the retro-deformation front, the size of the step will vary from zero to no more than half the total convergence. For simplicity we make the assumption that convergence is distributed uniformly across the orogen.

### *Surface Process Model*

To investigate the topographic response to uplift and shortening of an orogenic wedge, we use surface velocity fields provided by the tectonic model as a source function for a surface process model (SPM). The SPM we use is a modified version of the CASCADE code (Braun and Sambridge, 1997). This code is based on an irregular grid of points connected by a Delauney triangle algorithm (Braun and Sambridge, 1997). Physical surface processes are described mathematically to solve for changes in surface height on the grid. This algorithm has the advantage that grid nodes can be placed arbitrarily so can be moved to track tectonic surface displacements

Two surface processes are used in this version of CASCADE: diffusion of hillslope topography and incision of bedrock in fluvial channels (fig. 2). Diffusion is used to represent a variety of surficial hillslope processes not explicitly modeled, including regolith creep and mass wasting by bedrock-involved landslides. Diffusion in two dimensions, $x$, $y$, describes the timedependent change in height, $h$, of topography according to:

$$\frac{\partial h}{\partial t} = k_d\left(\frac{\partial^2 h}{\partial x^2} + \frac{\partial^2 h}{\partial y^2}\right) \tag{2}$$

with $k_d$ as a diffusivity (dimensions of length squared per time, $L^2/t$) representing the diverse and scale-dependent, physical properties mentioned above.

Fluvial processes operate on a river network constructed by collecting precipitation and integrating it down the path of steepest descent. Precipitation in all models of this paper is applied at a constant rate in space and time so that discharge is equivalent to upstream drainage area. River channels are defined by nodes that have a discharge $Q$ (dimensions $L^3/t$) greater than some threshold value, $Q_c$. Channels are determined to be either bedrock or alluvial based on a stream-power sediment capacity law:

$$Q_c = k_a Q \frac{\partial h}{\partial l} \tag{3}$$

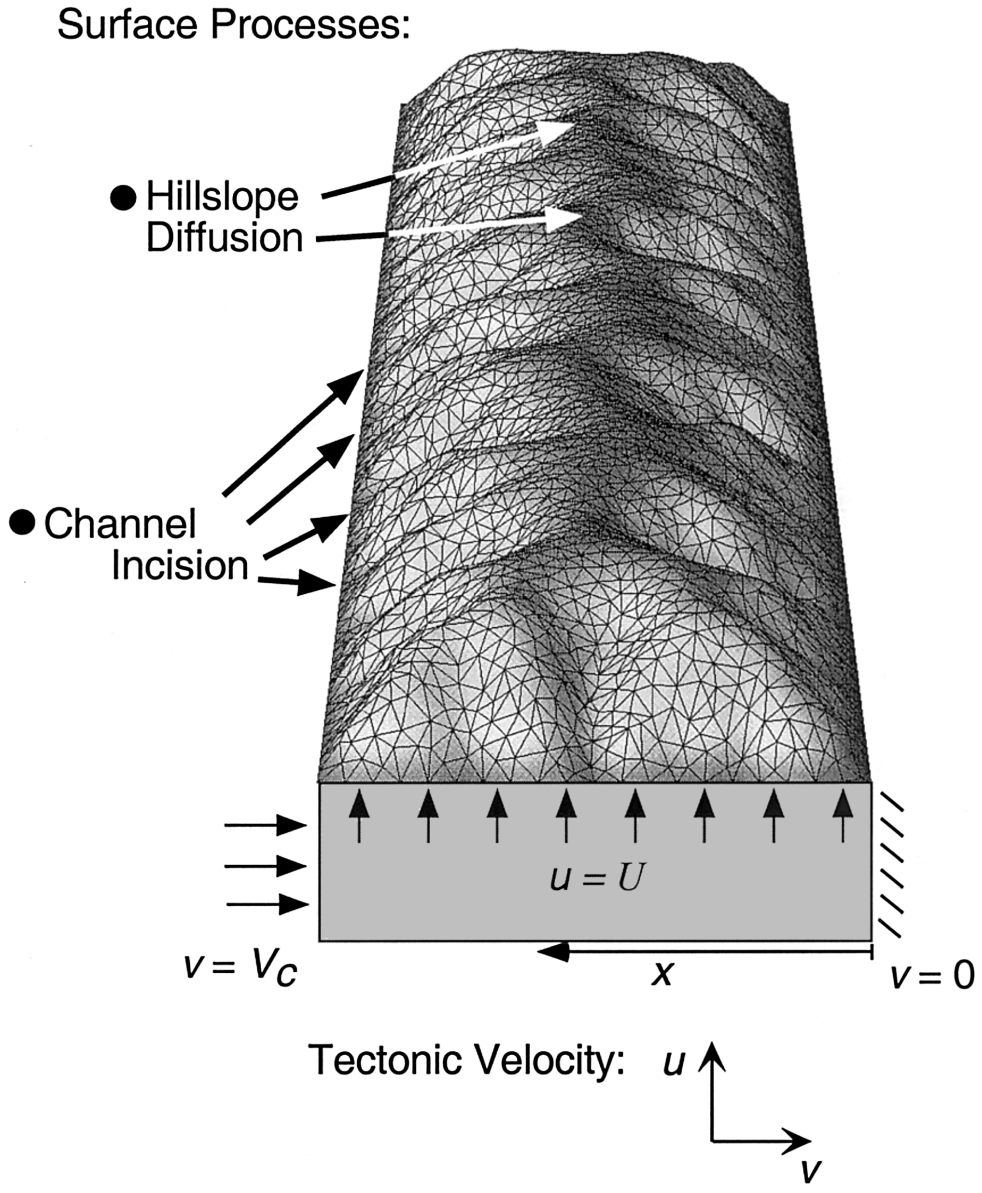


Fig. 2. Components of the coupled tectonic, surface process model. Surface velocity has vertical and horizontal components dictated by model of figure 1. Uplifted surface is eroded by hillslope diffusion and fluvial channel incision processes. The irregular grid used in calculations is shown, although new elements are added by frontal accretion. Boundary conditions for model are fixed elevation on all four sides. Model has aspect ratio of 5 to 1 to avoid edge effects and thus simulate two-dimensionality.

where $Q_c$ is the sediment carrying capacity expressed with dimensions of $L^3/t$, $\partial h/\partial l$ is the local bed slope, and $k_a$ is a dimensionless proportionality constant. Alluvial channels are defined as those carrying a sediment flux equal to the local carrying capacity. Bedrock channels have a sediment load less than capacity and thus have no sediment storage on the bed. They incise at a rate $\partial h/\partial t$, also taken to be proportional to stream power:

$$\frac{\partial h}{\partial t} = \frac{k_f}{w} Q \frac{\partial h}{\partial l} \tag{4}$$

where $w$ is the channel width, and $k_f$ is a proportionality constant reflecting the erodibility of the substrate and has dimensions of $1/L$. The channel width is taken as proportional to the discharge and, insofar as bedrock channels are similar in geometry to alluvial channels, is assumed to be proportional to the square root of discharge:

$$w = a\sqrt{Q}. \tag{5}$$

This introduces another proportionality constant $a$, with dimensions of $\sqrt{t/L}$. If the sediment flux in a channel exceeds the capacity of the river, sediment will be deposited so that the flux is maintained at capacity, that is, the channel aggrades, although in the models presented here, high uplift rates preclude the formation of alluvial channels.

Combining the two erosion mechanisms with an uplift, $u$, and a horizontal velocity in the $x$ direction of $v$ gives an equation for the change in height:

$$\frac{\partial h}{\partial t} = u + v\frac{\partial h}{\partial x} + k_d\left(\frac{\partial^2 h}{\partial x^2} + \frac{\partial^2 h}{\partial y^2}\right) + \frac{k_f}{a}\sqrt{Q}\frac{\partial h}{\partial l} \tag{6}$$

For the tectonic model described above, the vertical component of surface velocity is constant with a value, $U$, and the horizontal velocity is given by: $v = V_c x/L$, although $V_c$ must be defined as the velocity of the toe of the wedge, not the plate convergence velocity, so as to take into account the possibility of underplating. Thus, $V_c$ may vary between zero and the actual plate convergence velocity and is a primary free parameter in our modeling study. We reduce the model equations to a dimensionless form using $L$ and $U$ as scaling parameters. Non-dimensional variables are thus:

$$h^* = \frac{h}{L},$$

$$x^* = \frac{x}{L},$$

$$u^* = \frac{u}{U},$$

$$v^* = \frac{v}{U},$$

$$Q^* = \frac{Q}{UL^2},$$

$$t^* = \frac{tU}{L}.$$

Using the specific horizontal velocity function, we obtain the dimensionless transport equation:

$$\frac{\partial h^*}{\partial t^*} = u^* + \frac{V_c}{U}x^*\frac{\partial h^*}{\partial x^*} + \frac{k_d}{LU}\left(\frac{\partial^2 h^*}{\partial x^{*2}} + \frac{\partial^2 h^*}{\partial y^{*2}}\right) + \frac{k_f L}{a\sqrt{U}}\sqrt{Q^*}\frac{\partial h^*}{\partial l^*}. \tag{7}$$

There are three non-dimensional groups in this equation:

$$R = \frac{V_c}{U},$$

$$D = \frac{k_d}{LU},$$

$$N_e = \frac{k_f L}{a\sqrt{U}}, \tag{8}$$

which give the final version of the transport equation:

$$\frac{\partial h^*}{\partial t^*} = u^* + Rx^* \frac{\partial h^*}{\partial x^*} + D\left(\frac{\partial^2 h^*}{\partial x^{*2}} + \frac{\partial^2 h^*}{\partial y^{*2}}\right) + N_e\sqrt{Q^*}\,\frac{\partial h^*}{\partial l^*}. \tag{9}$$

*2.3 Numerical Experiments.*—The models presented in this paper comprise a series of numerical experiments illustrating the response of the topographic system to the tectonic "forcing" provided by accretion and uplift. The models are kept simple in order to isolate processes and the effects of specific parameters. The three non-dimensional groups in (9) serve as the primary parameters for these experiments. The threshold discharge for channel formation, $Q_t$, and the sediment carrying capacity coefficient, $k_a$, are set to low and high values, respectively so as not to play an important role in any of the models presented here. Each of the three non-dimensional parameters has a clear physical interpretation. The parameter $R$ is the ratio between the maximum horizontal velocity and the uplift rate and thus directly reflects the importance of frontal accretion relative to underplating with a value of 0 representing complete underplating and non-zero values reflecting a component of frontal accretion. $D$ is the inverse of the conventional Peclet number representing the relative importance of diffusion to vertical uplift. Small values of D thus reflect a system dominated by uplift with little diffusion of uplifted topography; large D implies a diffusion-dominated landscape in which the form of uplifted topography is quickly "diffused" by hillslope processes. The parameter group $N_e$ is referred to as the erosion number. It reflects the efficiency of fluvial incision processes relative to tectonic uplift. The erosion number, $N_e$, is an important parameter in coupled tectonic, erosion systems in which fluvial incision processes dominate (Willett, 1999); large $N_e$ implies higher erosional efficiency of the fluvial incision processes.

The simplicity of this parameterization allows easy investigation of parameter space and provides simple illustrations of process interactions and influences, but, as with all modeling exercises, simplicity comes at the expense of direct applicability to the natural world. In this case, the most likely source of deviation from the natural system comes from the representation of the hillslope processes by diffusion, as diffusion does not provide a good mathematical representation of landslides, debris flows, or other hillslope processes thought to be important in high-relief settings such as convergent mountain belts. We will elaborate on this limitation in the discussion. In any case, the purpose of the models is to provide physical insight, not to make specific predictions for given mountain belts, so that, although we make comparison to natural systems, direct inference of parameter values can only be interpreted through the model simplifications.

## NUMERICAL MODEL RESULTS

We present here a suite of numerical experiments, conducted to explore the steady-state topography produced by combinations of the three non-dimensional parameters described above. The initial condition for all models consists of a horizon-

tal surface with a small component of random, "white" topographic noise. We apply temporally steady and spatially uniform precipitation throughout the model duration. At each timestep an increment of crustal deformation is computed, followed by an increment of redistribution of mass by surface processes.

Computations proceed until the system reaches topographic steady state, defined here as the state in which the longest-wavelength of the topography no longer changes with time. A strict definition of topographic steady state is that the topography of all points in the domain is constant with time, but this condition is rarely met, even in simple numerical models, leading us to use the weaker definition given above. The strict definition of steady state is applicable in the case of pure underplating, in that the elevation of every model grid node does reach a steady value, a result consistent with Kooi and Beaumont (1996). However, frontal accretion and horizontal motion introduce a complexity that precludes a strict condition of steady state. Frontal accretion implies the addition of new material along the left edge of the model, which corresponds to the accretionary toe of the orogenic wedge (fig. 1). As a result of this accretion, each material point in the model is moving from left to right in the model domain. Because the calculation grid (fig.2) is tied to material points, it is moving toward the right at each step of the model calculation. To keep the grid spacing from increasing excessively in the prowedge requires that new nodes be introduced at the left boundary of the model domain. In keeping with the philosophy of a random grid, new grid points are introduced with a random component to their position. Thus, both the advection of the existing nodes and the introduction of new nodes at each time step cause continuous, small-scale changes to the calculation grid. This makes the determination of steady state in models with $R > 0$ problematic. Therefore, we define steady state in such models with reference to the average cross-sectional form of the mountain range, rather than using the stricter requirement that every grid point remain at a constant elevation.

### *Underplating ($R = 0$)*

In an orogenic system in which all mass is added by underplating, there is no horizontal contraction of the surface so that the horizontal velocity is zero, and the velocity ratio, $R = 0$. This is an endmember situation equivalent to the case investigated by Kooi and Beaumont (1996). The topography predicted from the surface process model is shown in figure 3 as a function of non-dimensional time, $t^* = tU/L$. Since the surface uplift velocity is constant in space, elevation increases with time, initially producing a broad, flat plateau. However as the fluvial channels incise the plateau, relief increases, and the topography develops a characteristic form in which transverse rivers, pinned at a base level at the model boundaries, incise the uplift from all directions leaving a prominent ridge and water divide defining the crest of the range. The model topography reaches a steady state at approx $t^* = .02$ and is approximately symmetric about the main divide with a series of near parallel transverse river valleys incising the range.

At steady-state and given that $R = 0$, the local rate of mass removal by surface processes must be equal to the uplift rate. In channels, this condition requires that channel slope and discharge adjust to incise at the appropriate rate according to eq 4. However, in channel heads and on water divides, diffusion is the only mechanism operating to remove mass; there, the slope must change to compensate surface uplift and achieve a steady state. The steady state landforms and the time to reach steady state are thus functions of both diffusive and fluvial erosion processes as well as the uplift rate and domain size. The dependence on uplift rate and domain size is linear, so the time to steady state scales linearly and is expressed efficiently in terms of $D$ and $N_e$ (fig. 4). Fluvial incision is the dominant process in most cases, and so $N_e$ determines the time to steady state other than for small values of $N_e$ and large values of $D$; this latter condition implies dominance of the diffusive process in the

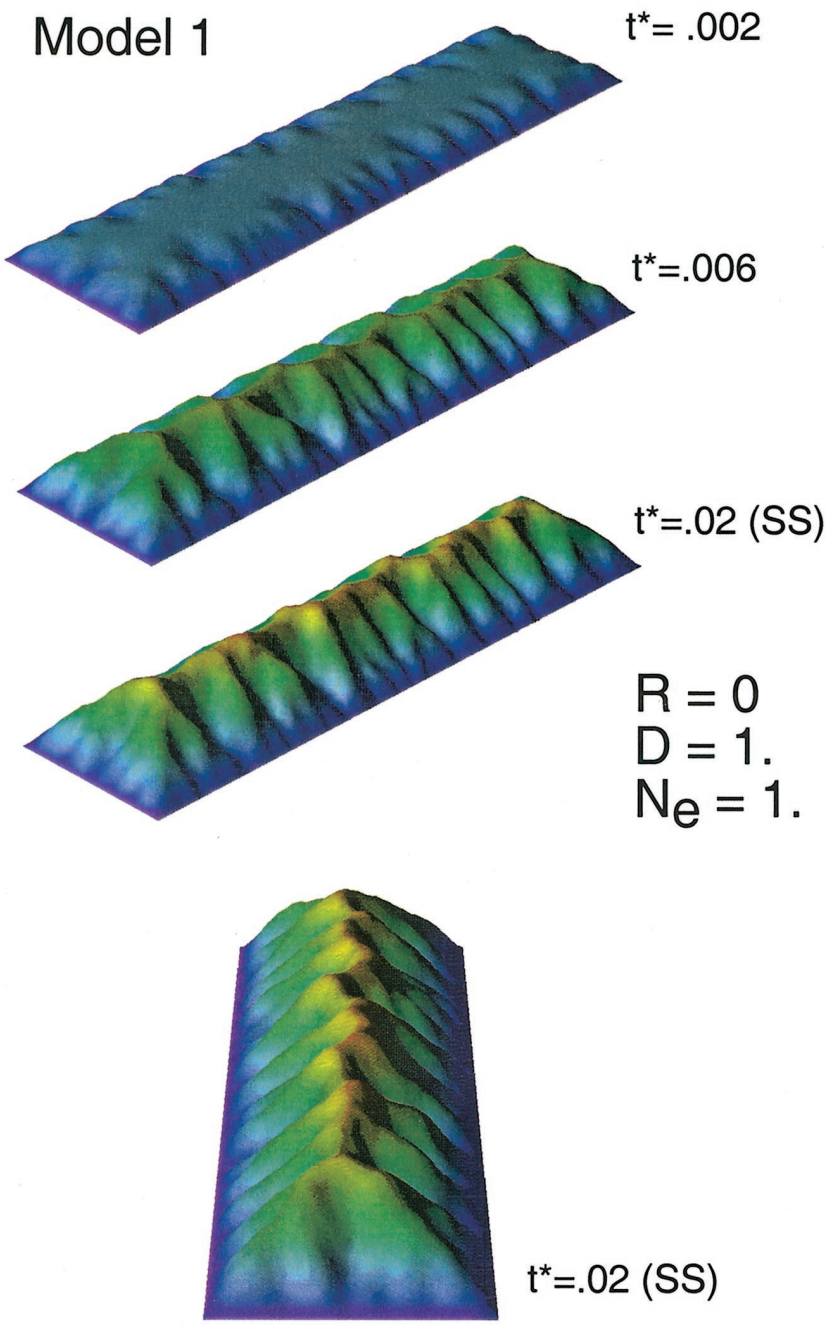


Fig. 3. Evolution of model topography with constant uplift rate and no horizontal velocity as a function of non-dimensional time, $t^* = tU/L$. Peclet number, $D$, erosion number, $N_e$, are 1.0. Steady state topography (lower two frames) is symmetric at the large scale and is reached at non-dimensional time of .02.

landscape, which is not typically applicable to active mountain belts and leads to unrealistic landscapes as demonstrated in a later section. Figure 4, like most of this analysis is non-dimensional, but for mountain belts with widths of 50 to 200 km,

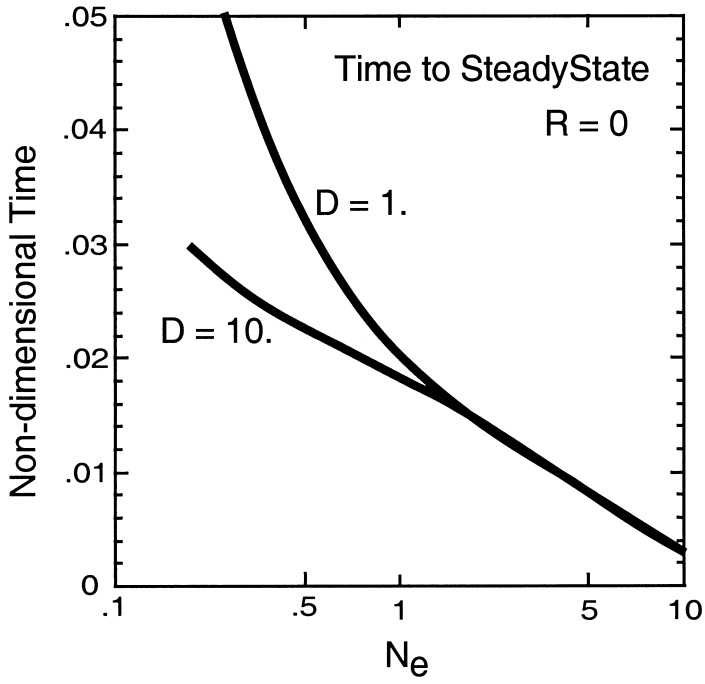


Fig. 4. Time required to reach topographic steady state for models with constant uplift rate and no horizontal velocity. Non-dimensional time ($t^* = tU/L$) is shown as function of erosion number, $N_e$, for Peclet numbers, $D$, of 1.0 and 10.

uplift rates of 0.1 to 1 mm/yr and $N_e$ and $D$ values of about 1, times to steady state would range from about 1 to 50 my, with the longer times applicable to the lower uplift rates.

*Horizontal Shortening ($R = 20$)*

Model 1 considered the topographic evolution of a mountain range in which internal kinematics were governed exclusively by tectonic underplating. Alternatively, if a significant fraction of the crustal mass is added to the orogen by frontal accretion, there will be a horizontal component to the surface velocity. This case is considered in model 2 (fig. 5) in which the velocity ratio, $R$ (eq 8) is specified as 20, and all erosion parameters are as in model 1. As a dimensional example of the velocity ratio, $R = 20$, consider a 100 km wide orogen uplifting at 1 mm/yr. For this configuration, the specified velocity ratio corresponds to frontal accretion of a 5 km thick section at a convergence rate of 20 mm/yr. Our tectonic model assumes a constant horizontal shortening rate, so the convergence velocity decreases linearly to zero across the orogen (eq 1). The most striking difference between model 1 (fig. 3) and model 2 (fig. 5) is the resultant asymmetry in the mountain topography. The horizontal component to the surface velocity gives rise to a migration of the main divide in the direction of the tectonic velocity (left to right in fig. 5). The topography at the scale of the entire mountain belt is thus asymmetric through its transient evolution and at steady state. In models with a horizontal component to the velocity field, the final elevation of the main divide is reached quickly, at approximately the time taken to reach steady state in symmetric models (fig. 4). However, after reaching its final height, the main divide continues to migrate in the direction of tectonic motion until it achieves its ultimate,

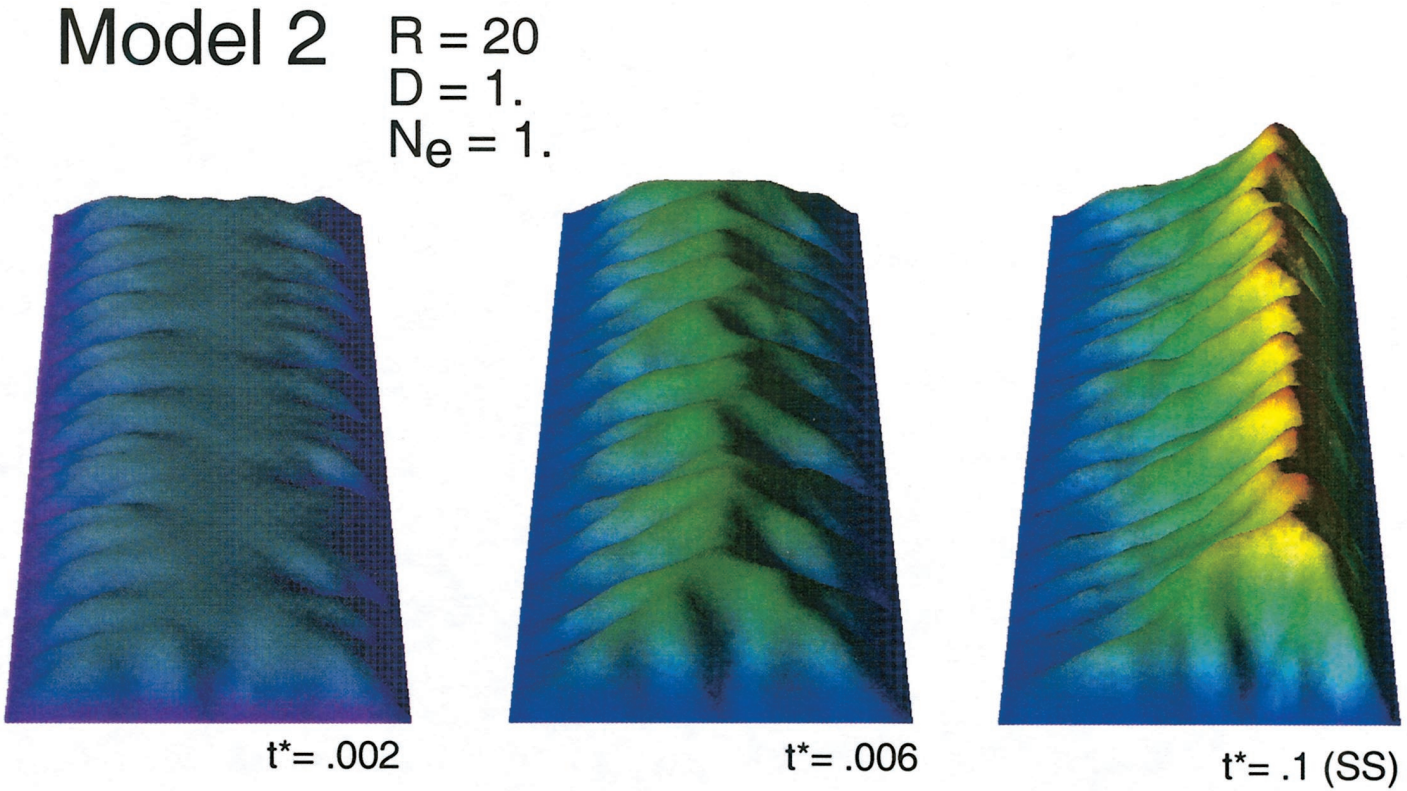


Fig. 5. Topographic evolution of model 2 which has a constant uplift rate of $U$ and a horizontal velocity gradient from zero at right edge to $20U$ at left edge, thus implying a velocity ratio, $R$, of 20. Peclet number, $D$, and erosion number, $N_e$, are both 1.0.

steady position after a period 5 to 10 times longer than the corresponding times for symmetric models. For example, model 2 (fig. 5) achieved steady state after about 0.1 dimensionless time units. This is about 5 times longer than in the corresponding model (model 1) without a horizontal velocity component.

A less striking, but nevertheless important consequence of horizontal shortening is a modification to the structure of drainage basins, and in particular to the slope-discharge product of the streams, or as is more often reported, the slope-area product. Numerous analyses of DEM data (Flint, 1974; Tarboton, Bras, and Rodriguez-Iturbe, 1991; Seidl and Dietrich, 1992; Rodriguez-Iturbe and others, 1992; Moglen and Bras, 1995; Maritan and others, 1996; Sinclair and Ball, 1996; Slingerland, Willett, and Hovius, 1998; Rinaldo and Rodriguez-Iturbe, 1998; Hurtrez and others, 1999; Whipple and Tucker, 1999; Snyder and others, 2000) have shown that the product $Q^{\alpha}S$ is relatively constant along any particular stream, but among streams $\alpha$, a measure of concavity, varies from 0.2 to 1.2. Conjectures on the origin of this variation range from variations in the bedrock erosion process to along-stream variations in uplift rate. Here we show that part of this variation in concavity can be caused by horizontal shortening. Consider a detachment-limited stream at steady state in which the channel axis is parallel to the $x$ direction, discharge increases linearly with distance downstream, and the bed erosion rate is given by eq 4. Then eq 9 can be rewritten as:

$$S(RTQ^* + N_e\sqrt{Q^*}) = u^*, \tag{10}$$

where $T$ is the ratio of the upward-directed rock flux per unit width to the unit water discharge per unit length of catchment. Eq 10 predicts that the product $Q^{\alpha}S$ will be constant along a stream at steady state, but the magnitude of $\alpha$ depends upon the relative magnitudes of $R$ and $N_e$. Larger values of $\alpha$ may reflect streams responding predominately to horizontal shortening.

### $N_e$-$D$ Parameter Space

The velocity ratio, $R$, is clearly an important parameter to the large-scale morphology of mountain belts, particularly to the across-strike asymmetry. However, we would also like to determine the importance of the non-dimensional groups $D$ and $N_e$, representing the scaled value of the diffusivity and the fluvial incision parameter, respectively. In practice only a narrow range of values of $D$ and $N_e$ produce reasonable mountain range topography. To illustrate this point we produced a series of models for a range of values of the Peclet and erosion numbers, $D$ and $N_e$, at a fixed value of the velocity ratio ($R = 20$). The resultant topography of these models defines distinct regions within the $N_e$-$D$ parameter space (fig. 6). Contours on figure 6 indicate the maximum elevation scaled by the width of the orogen. For example, the .005 contour represents a maximum relief of 500 m on a 100 km wide orogen. Very little elevation is implied for models in the upper, right field of figure 6, as the erosion processes remove nearly all excess topography. This is the case at very large $D$ ($>10$) or $N_e$ ($>10$) or, particularly, large $D$ and $N_e$. Depending on whether $D$ or $N_e$ is large relative to the other, the topography will be dominated by diffusion or fluvial incision. An example of a fluvially-dominated landscape with a large $N_e$ is given as model 5 in figure 7C. As noted, the maximum elevation is very small, and the landscape is highly dissected with little coherent structure to the drainage pattern. In contrast, model 3 in figure 7A represents the case of a landscape dominated by diffusion,with a Peclet number, $D = 10$ and an $N_e = .2$. Although a regional divide develops, the transverse drainage basins are barely incised into the uplifted region, and diffusion fluxes are responsible for nearly all the mass transport out of the model domain. Although such a diffusion-dominated topographic model might be applicable for some small-scale problems (small L), at the scale of a mountain belt, this morphology is clearly unrealistic. At

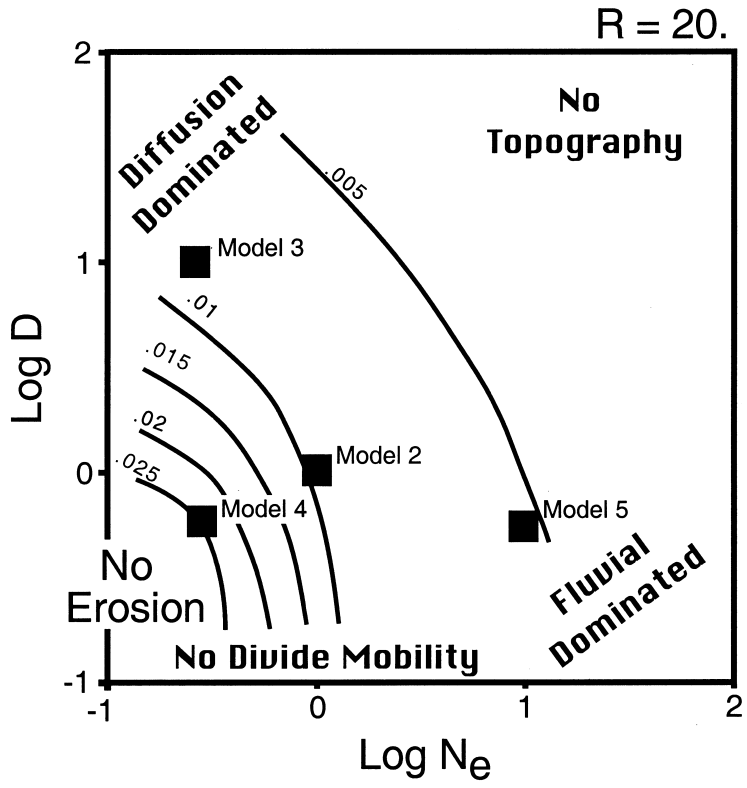


Fig. 6. Maximum elevation at steady state for models with velocity ratio, $R = 20$, as a function of Peclet number, $D$, and erosion number, $N_e$. Maximum elevation is scaled by model width, $L$. Parameter space location of specific models of this paper are indicated.

small $D$ and $N_e$, erosion rates are low, tectonic surface uplift dominates, and we obtain high topography (lower left corner of fig. 6). Model 4 (fig. 7B) is an example of a model with small $D$ and $N_e$. The resultant mountain belt is high, strongly asymmetric, and transverse rivers are not deeply incised. As with the other models in figure 7, this topography does not compare well with actual mountain belts.

Another important effect arises in models with low values of $D$. Since erosion of ridges can only occur by the diffusive mechanism, as diffusion decreases in efficiency, erosion of the ridges ceases to keep up with tectonic uplift and, more importantly, horizontal tectonic advection of the topography. This is very important to the position of the main divide ridge, which, in the complete absence of diffusion ($D = 0$), will uplift and move horizontally with the tectonic velocity, thereby precluding steady state topography.

### *Velocity Ratio, R, and Mountain Range Asymmetry*

The asymmetry of mountain range topography as characterized by the position of the main drainage divide is an important prediction of the surface process models. This asymmetry would not exist in the absence of horizontal tectonic motion, assuming other factors, such as climatic conditions and rock erodibility are symmetric about the ridge. Asymmetry in range topography thus implies a non-zero velocity ratio, $R$, and some component of frontal accretion and horizontal shortening. The quantitative dependence of range asymmetry on the other erosion parameters is less clear but can

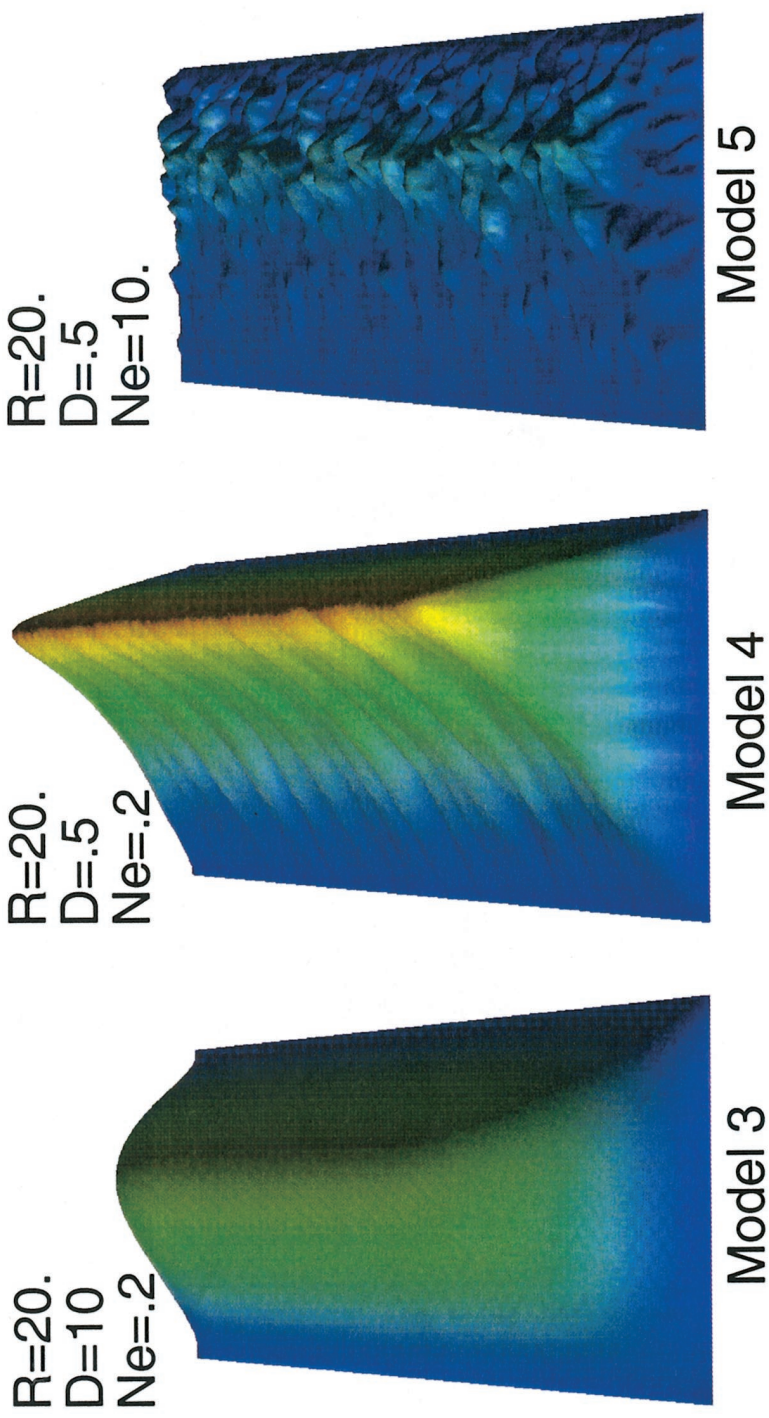


Fig. 7. Predicted steady-state topography for models with a velocity ratio, $R$, of 20, at various values of other erosion parameters. (A) Model 3 is diffusion dominated with $D = 10$ and $N_e = .2$. (B) Model 4 is uplift dominated with $D = .5$ and $N_e = .2$ C. Model 5 is dominated by fluvial erosion with $D = .5$ and $N_e = 10$. See figure 6 for maximum elevation and vertical scaling in each figure.

be established. As discussed in the previous section, the motion of the main divide and its final, steady state position should depend on the efficiency of diffusion as characterized by $D$, as diffusion is the only surface process operating on the model ridges. Tectonic advection of the topography tends to move the divide from left to right (figs. 5 and 7), and in the absence of ridge erosion, the divide would eventually end up on the extreme right side of the model domain. This motion is countered only by the diffusion of the ridge crest in the opposite direction. Steady state is reached when these two processes balance, that is when diffusive processes drive the ridge to the left at the horizontal tectonic velocity. In fact, the transient evolution of models with finite $R$, such as model 2 (fig. 5), is governed by that process. In these models, the asymptotic approach of the main divide to its final, steady state position, long after it has achieved its steady state height, reflects a balance between the opposing processes driving ridge migration. The dependence of range asymmetry on $R$ is expected and easily demonstrated by a series of models in which all parameters are held fixed, except $R$, which is varied systematically. Figure 8 shows the steady state topography for models with an $R$ of 0 to 20. For $R = 5$, there is a small, but significant, asymmetry to the topography. For $R = 20$, that asymmetry is extreme.

The dependence of asymmetry on $D$ can also be shown. The results from a series of such models is summarized in figure 9, which shows the range asymmetry as a function of both $R$ and $D$. Asymmetry is parameterized on the vertical axis in figure 9 as the fractional divide position which is simply the distance of the divide from the left (pro-) boundary, divided by the total domain width, so that 0.5 represents symmetry and 1.0 implies that the divide is at the right (retro-) boundary. As expected, $D$ strongly affects the steady state position of the range divide. Recall that $D = 10$ produces a diffusively dominated landscape (model 3), in which the low degree of asymmetry is the result of the large diffusion flux countering the tectonic advection. With no diffusion, $D = 0$, the ridge will migrate to the retro-boundary, producing a fractional divide position of 1.0 (top of fig. 9). No models were run to confirm this as it would be impossible to obtain meaningful numerical results for these conditions. The $D = 0$ line is therefore theoretical. For values of $D$ less than about 0.5, it is not clear when or if steady state is achieved, particularly at large $R$ which produces strongly asymmetric landscapes with steep slopes on the retrowedge. The $D = .1$ curve on figure 9 is dashed for this reason.

## NATURAL EXAMPLES

### *Orogenic Topography and Kinematics*

To demonstrate that these models have application to natural examples and to test whether we can use modern topography to constrain kinematic models of accretion by underplating or frontal accretion, we have compiled topographic and kinematic data from three modern, active orogenic systems, the Southern Alps of New Zealand, the Central Range of Taiwan, and the Olympic Mountains of Washington State. Each of these orogenic systems has been proposed to be in steady state. We summarize the observations from each below.

*Southern Alps of New Zealand.*—The Southern Alps of New Zealand is a young orogenic belt that has formed in response to ongoing oblique convergence between the Pacific and Australian plates (Walcott, 1978, 1998; Wellman, 1979). The relative plate motion through the South Island of New Zealand has a large transcurrent component of about 38 mm/yr compared to 13 mm/yr of convergent motion (Norris, Koons, and Cooper, 1990; Walcott, 1998). This plate motion is partitioned between slip on the range bounding Alpine Fault and distributed shortening in the Southern Alps (Walcott, 1978; Cooper and Norris, 1994). The distribution and mode of convergence at depth is more difficult to obtain. However, it has been proposed that convergence is

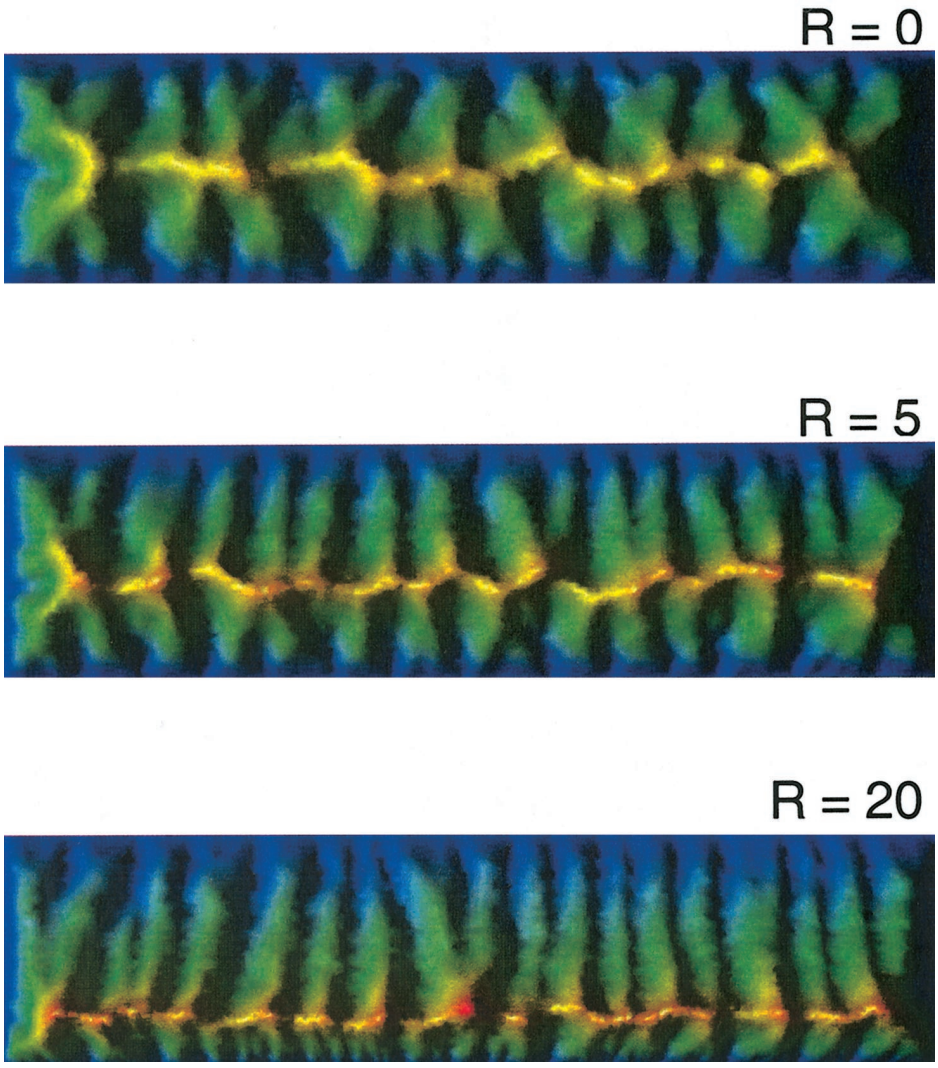


Fig. 8. Steady state topography as a function of velocity ratio, $R = V_c/U$. Top view shown. Note increased asymmetry in position of main water divide with increasing horizontal velocity, $V_c$.

achieved by mantle subduction and crustal accretion of Pacific plate (Wellman, 1979; Norris, Koons, and Cooper, 1990; Beaumont and others, 1996), so that subduction is down to the west, and the accretion of new material into the orogen is from east to west.

The best estimate of current shortening rates across the Southern Alps comes from recent GPS studies (Beavan and others, 1999). They report 10 to 11 mm/yr of total convergence across the orogen, although the uncertainties involved are significant and model dependent. There remains ambiguity in geodetic data in that displacements measured over periods shorter than the earthquake recurrence time could be in part, or entirely, elastic strain associated with the seismic cycle and thus could be unrepresentative of the geologic timescale strains. Beavan and others (1999) interpret the observed shortening in terms of a locked segment of the Alpine fault and

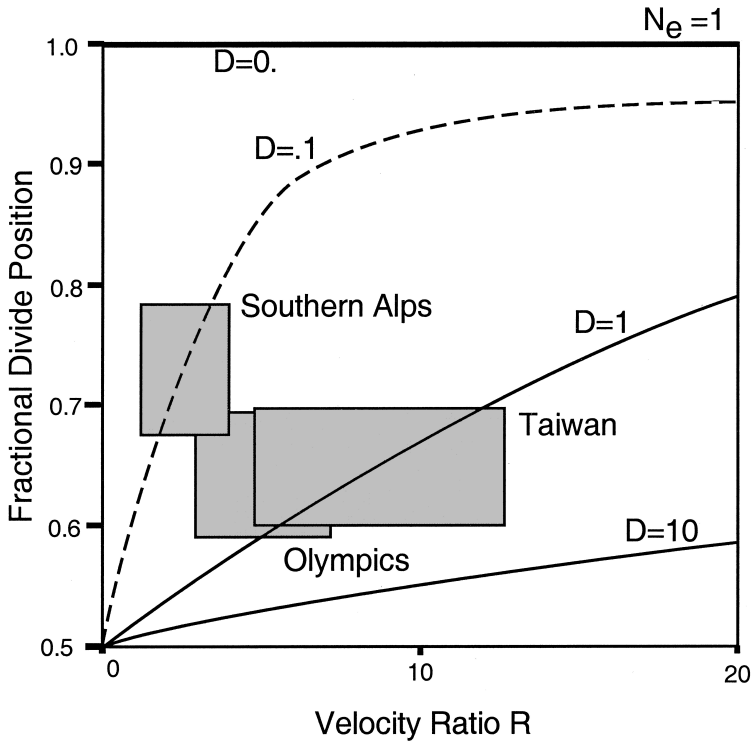


Fig. 9. Mountain range asymmetry as measured by steady state fractional divide position as a function of velocity ratio, $R$, and Peclet number, $D$, at a constant $N_e$ of 1.0. Curves were constructed by interpolating between multiple model runs such as in figure 8, except $D = 0.0$ (constant at 1.0) which is theoretical. $D = 0.1$ curve is dashed to indicate uncertainty as to whether steady state was achieved. Boxes indicate observed range asymmetry and velocity ratio from active mountain ranges as discussed in text.

concluded that 30 to 50 percent of the shortening was permanent strain of the upper plate; the remainder is taken up on the Alpine fault during large earthquakes. For our purposes, this strain partitioning represents a deviation from our assumption of constant strain rate, but it is the total horizontal shortening rate that is most important for comparison to the models.

Vertical surface uplift rates cannot be determined accurately by GPS methods and so must be inferred by other techniques. If the orogen is in steady state, estimates of exhumation rates can be used to infer rock uplift rates, and this method has been used in the Southern Alps. The assumption of steady state is justified by the high erosion rates observed in response to the harsh climate. High erosion and exhumation rates have been inferred by a number of studies, using different techniques (Walcott, 1978; Adams, 1980; Whitehouse, 1987; Kamp, Green, and White, 1989; Norris, Koons, and Cooper, 1990; Tippet and Kamp, 1993; Batt and Braun, 1997; Hovius, Stark, and Allen, 1997; Batt and others, 1999). Although erosion rates are highest on the west facing slopes of the range due to a strong, orographic forcing of precipitation rates, it is the net erosive flux by surface processes, that is important to the attainment of steady state (Koons, 1989; Willett, 1999). Uplift rates on the western side of the Southern Alps may reach a maximum of 11 mm/yr (Wellman, 1979; Tippet and Kamp, 1993; Batt and others, 1999), but, if the orogen is in steady state, the average erosive flux from the range implies an average vertical component to the surface rock velocity of 4 to

5 mm/yr (Walcott, 1998). Based on these estimates of the horizontal and vertical velocities, we estimate a velocity ratio, $R$ of between 1 and 4 for the Southern Alps with subduction down to the west.

The topography of the Southern Alps is strongly asymmetric with steeper regional slopes on the west side of the range. To illustrate this, we digitized profiles of the topography projected onto a section perpendicular to the average strike of the range (fig. 10A). Topographic profiles were derived from 1:50,000 scale maps. We determined the longitudinal profiles of major transverse rivers and interfluves independently; river profiles are concave-up in figure 10; interfluves are rougher and typically convex-up. Transverse rivers on the east side of the range do not all run perpendicular to the strike of the range, probably in response to transverse shear strain across the range as well as effects of local structure, so only one transverse river was digitized. Whether one focuses on river profiles or average topography, it is clear that the cross-sectional profile of the range is strongly asymmetric. The main divide is located at less than 30 km from the west coast and between 50 and 80 km from the east coast. This corresponds to a fractional divide position of .68 to .78.

*Central Range of Taiwan.*—The mountainous topography of Taiwan arises from the ongoing collision of the Luzon arc with the passive margin of Asia. This oblique collision initiated about 8 Ma in the north of Taiwan and has propagated to the south (Suppe, 1981). At present the offshore region south of Taiwan is thought to be in a pre-collision state. The Central Range down the axis of the island exposes the shortened, thickened, and exhumed crustal rocks of the main collision zone. In spite of the increasing age of the collision to the north, the average elevation and width of the Central Range does not increase along its northern two-thirds. This has led to the proposal that the range is in topographic steady-state (Suppe, 1981; Deffontaines and others, 1994), a conjecture supported by the observation of high erosional sediment fluxes and exhumation rates (Li, 1976; Liu, 1982; 1988; Hsieh, 1990; Tsao, 1993; Hovius and others, 2000).

The convergence rate between the Philippine Sea plate and the Asian plate in the vicinity of Taiwan is estimated at about 70 mm/yr (Seno and others, 1993), although recent GPS data indicate a slightly higher rate (82 km $Ma^{-1}$) (Yu, Chen, and Kuo, 1997). This relative plate motion vector is offset 10° clockwise with respect to the orthogonal to the mountain belt, so that relative plate motion is more orthogonal than in the Southern Alps. Currently, about 20 to 30 mm/yr of the convergence is taken up by shortening of the Philippine Sea plate and the Coast Ranges of eastern Taiwan. The Central Range is shortening at about 50 mm/yr. GPS studies (Yu, Chen, and Kuo, 1997) have demonstrated that the plate convergence is distributed broadly across the Central Range, although there is considerable complexity to the strain field, including local extension (Crespi, Chan, and Swain, 1996).

Numerous studies have documented the structural manifestations of the plate convergence. In particular, shortening in western Taiwan has led to the development of a thin-skinned fold-and-thrust belt forming by eastward underthrusting of the Asian crust beneath the orogenic belt (Suppe, 1981, 1984; Davis, Suppe, and Dahlen, 1983). This is consistent with the polarity of subduction to the south where the oceanic crust of the South China Sea (part of the Asian plate) is subducting down to the east beneath the Luzon Arc.

The vertical component of the tectonic uplift is more difficult to determine. Geodetic data suggest that the easternmost Central Range is uplifting at rates as high as 7.5 to 17.5 mm/yr relative to the Coast Range (Chen, 1984; Liu and Yu, 1990). Liu (1995) reports uplift rates as high as 35 mm/yr elsewhere in the Central Range. However these rates are likely to be associated with spatially or temporally anomalous tectonic events. Longer timescale sampling is provided by exhumation rates deter-

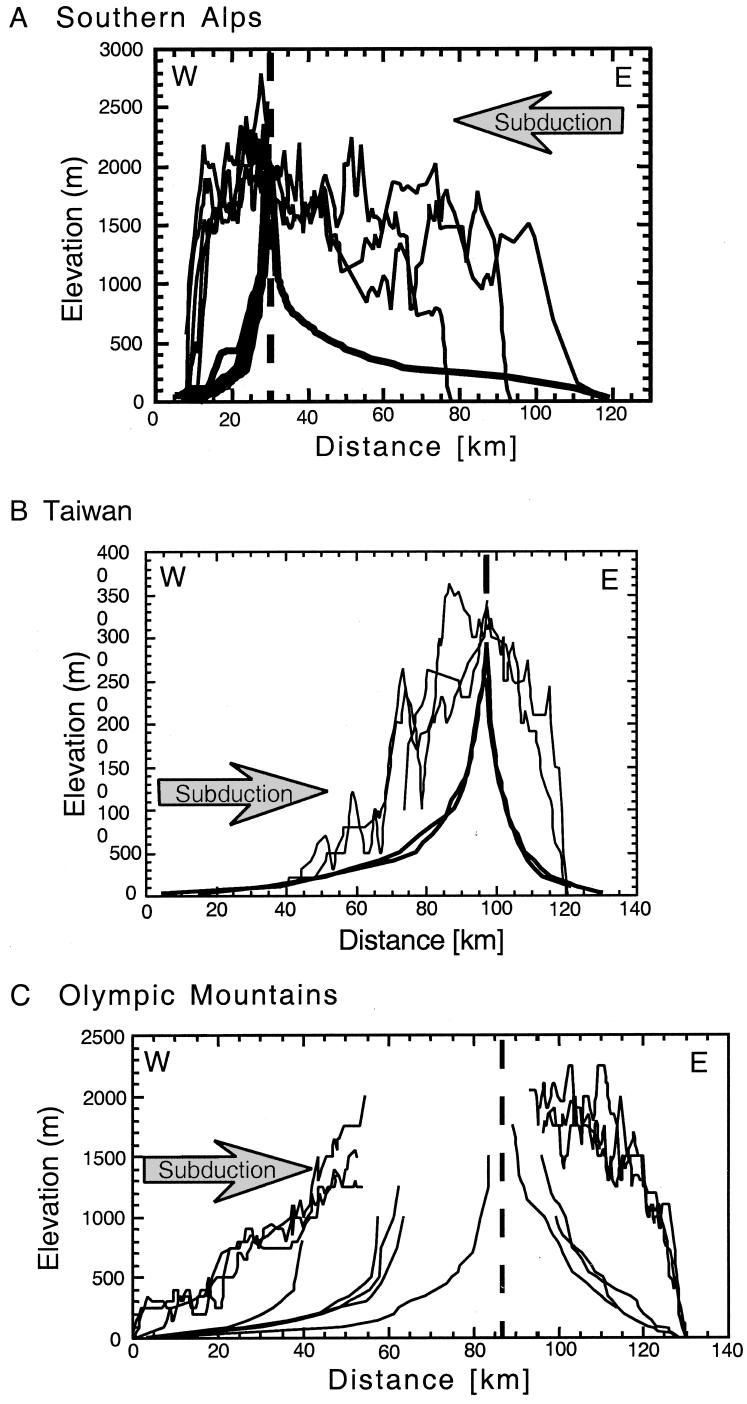


Fig. 10. Topographic profiles from: (A) Southern Alps of New Zealand, (B) Central Range of Taiwan, (C) Olympic Mountains of Washington State. Each figure shows projected longitudinal profiles of transverse rivers (concave-up curves) and profiles of interfluvial ridges. Olympic Mountains have a near-circular shape so that drainages are shorter to the north and south; profiles are aligned at base level.

mined from thermochronometers, although their use requires assuming steady-state. Zircon fission track studies (Liu, 1982; Hseih 1990; Tsao and others, 1993; Tsao, 1996) yield ages as low as 1 Ma in the eastern Central Range and imply exhumation rates of about 5 mm/yr, given the high geothermal gradients typical for the region. Apatite fission track ages from gneisses of northeast Taiwan (Liu, 1982) are typically under 1 Ma, consistent with exhumation rates on this order. Based on these lower uplift rates and the GPS-determined horizontal shortening rate, we estimate a velocity ratio, $R$, of between 5 and 12.5 for the Central Range (fig. 9).

The topography of the Central Range is characterized by high relief of up to 4000 m and deeply incised transverse rivers. The main divide of the Central Range runs north-south along the axis of the island, separating the steeply dipping east flank of the mountain belt from the shallower west flank: at the large scale, the mountain belt is asymmetric in cross section. This asymmetry is illustrated by the series of profiles in figure 10B, again obtained by projecting digitized topography onto a section in the direction of convergence. Transverse rivers are well defined and nearly identical in form on the eastern range flank; there are six rivers superimposed on figure 10B. Fewer rivers drain the mountain belt to the west. They run more obliquely to the range, apparently entrained in local structures. Only two of these rivers are shown in figure 10B.

*Olympic Mountains of Washington State.*—The Olympic mountains are a part of the series of mountain ranges from the Klamaths of northern California to the Insular Range of Vancouver Island that define the forearc high of the Cascadia subduction zone. This forearc high represents the topographic and structural apex of an accretionary complex that has formed from off-scraped sediments of the Juan de Fuca plate (Tabor and Cady, 1978). In the Olympic mountains, the metamorphosed sediments of the accretionary wedge have been deeply exhumed in contrast to the rest of the continental margin. This deeper exhumation is attributed to a longer phase of sub-aerial exposure and erosion (Brandon and Calderwood, 1990; Brandon, Roden-Tice, and Garver, 1998). Unlike the two previous examples, there is no collision between continental crust on separate plates. The mountain-forming process is one of accretion of sediment from a subducting oceanic plate. For this reason, the uplift rates are less than in the examples from Taiwan and New Zealand, but the process is still one of accretion, shortening, crustal thickening, and uplift with a kinematic model that potentially includes horizontal as well as vertical components.

Fission track studies of both zircon (Brandon and Vance, 1992) and apatite (Brandon, Roden-Tice, and Garver, 1998) suggest that exhumation of the deep accretionary wedge has occurred at a near-constant rate of just under 1 mm/yr since initial emergence between 12 and 17 Ma. The consistency of this rate derived from multiple thermochronometers supports the premise that the erosion rates are in steady-state, and insofar as erosion rates depend on the topography, the topography is also inferred to be in steady-state. Brandon, Roden-Tice, and Garver (1998) inferred a spatial pattern to exhumation rates with the highest rates observed at high elevation in the core of the range and rates decreasing to near zero at sealevel. With the assumption of steady-state, the inferred exhumation rate can be used as the vertical component of the tectonic velocity, and in keeping with our assumption of spatially constant uplift rate, we use the mean value of 0.8 mm/yr.

The horizontal component of the tectonic velocity can be determined from geodetic data. Khazaradze, Qamar, and Dragert (1999) present GPS data for the Cascadia margin. Although there were no stations directly outboard of the Olympic mountains, they found that the coast, north and south of the Olympics, is moving toward stable North America at a velocity of about 10 mm/yr and in the direction of the relative plate motion. However, west coast GPS stations are influenced by elastic

strains associated with subduction zone earthquakes, and Khazaradze, Qamar and Dragert (1999) demonstrated that 70 to 100 percent of the measured velocity could be due to elastic strain buildup in anticipation of a major earthquake. Another estimate of the shortening rate can be obtained by assuming steady state and considering the mass flux that must occur across the coast in order to balance the erosional flux out of the Olympics. The accretionary wedge is approx 20 km thick at the coast, so to balance the erosional flux across the 80 km wide range, the velocity ratio, $R$, must be about 4. Note that this estimate of $R$ is independent of the uplift or erosion rate. However, it is a maximum estimate in that it assumes no underplating. The minimum value for $R$ is difficult to constrain. In principle, the entire wedge could be growing by underplating so that $R$ is zero. However, this seems unlikely given the spatial pattern of deeper exhumation toward the east of the Olympic core, and Pazzaglia and Brandon (2001) and Batt and others (in press) argue that deformation is dominated by frontal accretion.

Topographic relief in the Olympics is significant if not extreme. Peak elevations in the Olympics are typically about 2.5 km, and local relief is due, at least in part, to recent glaciation. The limited north-south extent of the range results in an almost radial drainage pattern. However, with the exception of the Elwa river which runs north to the Straits of Juan de Fuca, the major rivers drain to the west. The east slopes are incised by a series of steep valleys draining to Puget Sound. Rivers on the western slope have different basin lengths reflecting the changing distance to base level from north to south. For this reason, projected topographic profiles are of significantly different lengths, making comparison difficult (fig. 10C). Nonetheless, all river longitudinal profiles show the same concave-upward form on both sides of the range. The large-scale topography is clearly asymmetric as, with the exception of the very shortest basins to the north and south, all west-draining basins are longer than the eastern counterparts.

### *Analysis of Observations in Context of Model Results*

The three examples of active orogens presented above all show significant asymmetry in their across-strike topographic form (fig. 10). This asymmetry is consistently correlated with the polarity of subduction (fig. 10), so that in each case the retrowedge is steeper and shorter than the matching prowedge (fig. 1). Independent of the condition of steady-state, this suggests that the topography of these examples is strongly influenced by horizontal shortening, or more specifically, the shortening associated with unidirectional accretion of new crustal material, consistent with our model results.

This conclusion differs from earlier workers who attributed orogen asymmetry to differential erosion on opposing sides of mountain belts due to prevailing wind patterns and orographic precipitation effects (Barry, 1981; Koons, 1989; Beaumont, Hamilton, and Fullsack, 1992; Willett, 1999). Orographically increased precipitation increases river discharge, fluvial incision, valley lowering, and headward channel incision relative to a dry climate. The result for an uplifting mountain range with orographic climate asymmetry and no horizontal tectonic motion would be an asymmetric topographic section with the wet side exhibiting longer valleys thus forcing the main divide toward the dry side of the range. Although investigation of climate effects are beyond the scope of this paper, one expects that climate-induced asymmetry could be as significant as tectonically induced asymmetry.

The relative roles of tectonic advection and asymmetric precipitation can be tested using the three mountain belts discussed above. Two have strong orographically induced asymmetry in precipitation. The exception is Taiwan, which has an orographically influenced climate with high precipitation rates in the mountains, but the rates are not asymmetrically distributed because of the weather patterns which include a

summer monsoon from the southwest, a winter monsoon from the northeast, and typhoons which can approach the island from any direction. In contrast, the Southern Alps and the Olympics both have dominant weather systems that approach from the west producing a wetter west side and a dryer east side. For the Olympic mountains this produces an ambiguity in the cause of the topographic asymmetry in that subduction is down to the east, so that the prowedge tapers to the west and receives the highest rates of precipitation. Thus both climate and the tectonic motion tend to force the range divide to move to the east contributing to the observed asymmetry (fig. 10C). The Southern Alps are the more interesting case in that the climatic asymmetry is opposite to the tectonic forcing, which results from down to the west subduction, so that the retrowedge receives the high precipitation. Climatic forcing and tectonic forcing are thus in direct competition with respect to migration of the main range divide. In spite of this competition, the Southern Alps show the largest asymmetry of the three examples, with the polarity of the topography clearly supporting the tectonic motion as the dominant mechanism (fig. 10A).

In addition to the offset position of the main water divide, the longitudinal form of the interfluves also shows systematic variation with the polarity of subduction. Interfluves on the side of the range facing the subducting plate are commonly linear or even slightly concave upward, whereas interfluves on the opposite side are uniformly convex upward (fig. 10). This morphology is also observed in the surface process models (figs. 5 and 8) and is likely a function of the horizontal advection of topography in the direction of subduction. The horizontal component of the surface displacement will tend to increase relief in the direction of motion on the retrowedge where the toe of the interfluve is pinned to its baselevel at the deformation front. Although the surface process models do not include landslides and therefore cannot address this issue directly, we speculate that these interfluves are steepened to the point of failure and held there by the combination of ridge migration, uplift, and horizontal advection, all of which tend to increase the relief of the interfluve. In contrast, on the prowedge, the uplift of the interfluves is in competition with their migration toward the orogen interior. If advection is fast enough, interfluves advect inward faster than relief is created by uplift and thus are not likely to be at their failure limit.

The model results showed that topographic asymmetry should increase with velocity ratio, assuming all other factors are equal. This relationship is not obvious in figure 9, and, if the three mountain belts show any trend, it is the converse. Possibly the relationship is obscured by varying $D/N_e$ ratios, although it is not obvious why diffusive processes in the Olympic range would be relatively less important than in Taiwan. What can be said is that the three orogens all plot primarily in the field of Peclet numbers between 0.1 and 1. As argued before, this is the zone in which diffusive processes at the drainage divide are strong enough to stop advection of the ridge but weak enough (relative to stream erosion) to produce realistic topography. From that perspective, the observations are consistent with our interpretation that divide position is a function of velocity ratio.

## DISCUSSION

### *Parameters Controlling Steady-State Morphology*

The surface process models used here provide a simple, but useful analysis of the parameters controlling the timing and form of topography as it evolves to a steady state in response to tectonic uplift and horizontal strain. Each of three non-dimensional parameters, $R$, $D$, and $N_e$, used to characterize the system, plays a role in the evolution and the final character of the topography. The erosion number, $N_e$, controls to a large extent the final character of the landscape in terms of the scale of topography and the relief. Since $N_e$ reflects the erosional efficiency of the fluvial system, which dominates

the overall mass removal of the surface processes, high $N_e$ implies low maximum elevation and low-relief topography, although the smaller scale relief and drainage density also depend on the diffusional efficiency characterized by $D$. In addition, the erosion number also determines the time required to reach steady state in the case of an exclusively vertical tectonic velocity field.

The situation is significantly different if the tectonic velocity field has a horizontal component. Then, the topography reaches its maximum height at approximately the same rate as with the vertical velocity field, but steady state is not achieved until the main divide has migrated to the point that asymmetry in the diffusional flux balances the horizontal tectonic velocity. Because the ridge position is determined exclusively by diffusion and the tectonic velocity, it is the Peclet number, $D$, and the velocity ratio, $R$, that largely control both the time to steady state and the final form of the topography. The role of the velocity ratio in this respect is clear (fig. 8): the larger the horizontal velocity relative to the uplift rate, the greater the degree of asymmetry to the steady-state range.

The effects of the diffusion parameter, $D$, are also pronounced (fig. 9) but more complex. Diffusion is the only surface process included in this model capable of eroding the ridge tops. The model ridge crests therefore can move only if one ridge flank erodes faster than the other. With diffusion this occurs exclusively if one side of the ridge is steeper than the other. Thus, it is the preferential steepening of one side of the ridge that becomes the necessary condition for steady state. Reality may differ considerably from this simple model. In particular, diffusion is not necessarily the most appropriate mathematical expression for surface processes eroding high ridges in active mountain belts. Bedrock landslides, mass wasting, or even cirque glaciers might play important roles in eroding ridges, and these processes may not be simulated well by diffusion (Densmore, Ellis, and Anderson, 1999; Ellis, Densmore, and Anderson, 1999). This is an important limitation to the SPM presented here. Diffusion is a simple parameterization, but if it is not representative of the actual surface processes, the quantitative results presented here must be interpreted with caution. However, in spite of the limitations of the model, the physical processes and qualitative behavior of the system are likely to be robust. Tectonic advection of topography must result in a degree of topographic asymmetry, moderated only by the surface processes active at ridge divides. If the dominant process there is not diffusion, some other mechanism will take its role to determine the ridge mobility. In general there will be some parameter equivalent to the Peclet number $D$ in figure 9, which will express the geomorphic mobility of the ridge, so that although the functions in figure 9 might change in detail, the inference that ridge mobility affects range asymmetry should be robust.

### *Ridge Migration and Drainage Capture*

Advective ridge migration during the approach to steady-state has the potential to derange significantly orogen drainage. In our models with horizontal motion the ridge migrates toward the retro-deformation front (left to right in fig. 5), in the direction of tectonic motion. However, this motion is in a spatial reference frame, that is, it is relative to an outside observer who is fixed to the domain boundaries. The material points at the ridge are moving with the tectonic velocity, which is always larger than the ridge migration rate. This implies that in a local frame-of-reference, fixed to a material point, it would appear that the ridge is migrating in the opposite direction toward the pro-deformation front (right to left in fig. 5). It is this frame-of-reference that is appropriate to geomorphic observations. In particular, if the ridge migration occurs in discrete jumps by drainage capture across the main water divide, this should result in the drainage divide jumping toward the tectonically accreting (pro-) boundary. Thus, the observation of a water divide jumping in one direction by drainage basin capture might actually be representative of the divide moving in the opposite direction relative

to its basin discharge point. There is a potential example of this in the Southern Alps of New Zealand where the westward draining Landsborough River runs parallel to the main divide. Eventually, this stream drains into one of the major transverse rivers that characterize the western flank of the mountain belt. High-order lateral drainage is rare in the western Southern Alps, but several large, lateral rivers drain the drier east flank of the range. A wind gap separates the Landsborough from one of these east-draining rivers. It is likely that the Landsborough is a drainage element of east flank origin, captured by a west-draining, transverse stream, as it was advected toward the Alpine fault (Koons, 1995).

There are also implications for the drainage pattern that develops on opposing sides of a mountain belt. On the prowedge, longitudinal foreland rivers or streams that are entrained by structures in the frontal regions of the orogenic wedge will be advected farther into the range with time. On the retrowedge, advection moves material from channel heads toward the discharge point, so there is little opportunity for lateral river capture or advection. This could lead to pronounced differences in drainage pattern between range flanks, particularly when the accreting prowedge is an on-land fold-and-thrust belt with large, longitudinal structures that exhibit high uplift rates while active. There is evidence for this in both Taiwan and New Zealand, where transverse rivers are uncommon on the prowedge. Instead, rivers run oblique to the trend of the range and are associated with individual structures. On the retrowedge, the drainage pattern is characterized by parallel, transverse river catchments oriented perpendicular to the range trend.

### *Scale Dependence of Steady State*

In light of the foregoing model results and observations, the definition of topographic steady state deserves more discussion. The strict definition of topographic steady state is that the topography (elevation) is unchanging with time at all points in a landscape, provided steadiness of all externally imposed conditions including horizontal and vertical velocity, climatic conditions, and physical properties of the surface processes. One can argue about how steady these conditions are in the natural world, but the numerical models can certainly simulate steady forcing, and such models would be expected to produce perfect topographic steady state. This is indeed the case for models without horizontal velocity (fig. 3), which evolve to a state in which every model node has a constant elevation. However, models with horizontal tectonic velocity are not so simple. Without horizontal motion, steady state at a spatial point is achieved when the uplift rate and the erosion rate are equal. With a horizontal component to the velocity, there are three rates that must sum to zero for steady state: the uplift rate, the erosion rate, and the horizontal mass advection rate which is given as the scalar product of the horizontal velocity and the surface slope. In practice this condition might be nearly impossible to achieve because of the variability in surface slope orientation. Any natural topography will have slopes that dip in virtually all orientations. In a uniform strain rate field, the horizontal velocity will have a constant direction, although the magnitude will vary. The change in elevation of a spatial point due to advection will thus vary depending on the orientation of surface slope. In order to achieve steady state, slopes of different orientations must erode at different rates. In particular, at steady-state, slopes dipping toward the accreting boundary of the prowedge (upstream to the tectonic flow) would need to erode slower than those dipping away from the accreting boundary. Thus, to maintain steady-state, the magnitude of slope must vary systematically with orientation, a characteristic highly unlikely to be met at all scales in a landscape.

To illustrate the problematic nature of this requirement, we consider a high order tributary on the side of a transverse interfluve such that the tributary runs parallel to the main divide and perpendicular to the direction of tectonic advection. If the

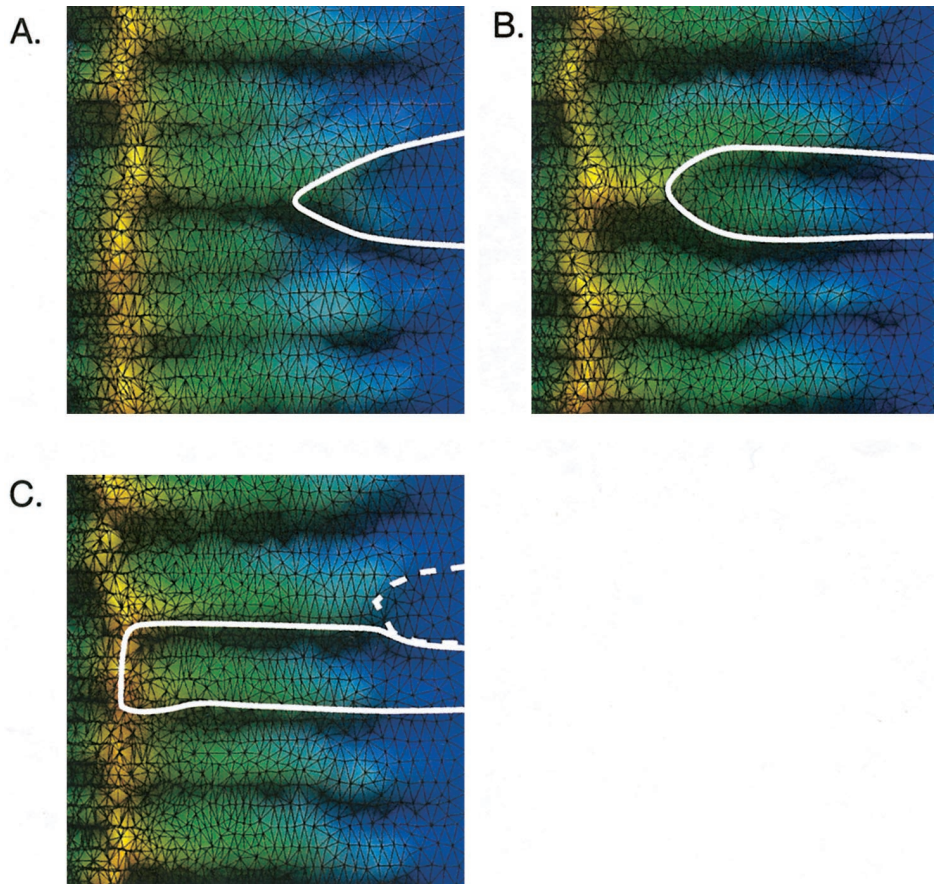


Fig. 11. Destabilization of an interfluve by tectonic advection which is moving material from right to left. Model topography, lit from top of page, is given with progressive time from (A) to (C). White line indicates a single drainage basin growing with time by a process of splitting of an interfluve. In C, process has initiated again as indicated by basin denoted by dashed line.

topography is in steady state, the tributary must remain fixed in a spatial reference frame. To do so requires that it incise laterally at the same rate as the tectonic velocity and in the opposite direction, that is, upstream to the tectonic flow. This in turn requires a strong topographic asymmetry to the tributary valley sides. Such a topographic asymmetry would have to exist for all features and at all scales in the landscape in order for perfect steady state to be achieved. This is highly unlikely to be the case.

Unsteadiness of topographic features parallel to the horizontal motion is evident in the models. The main interfluves separating transverse rivers do not stabilize in the models, even after the main divide appears to be fixed in height and position. An interesting phenomenon occurs to destabilize the interfluves and is illustrated in figure 11. Small channels on the end spurs of the interfluves are unable to stabilize with the tectonic advection and thus tend to grow toward the main divide as the channel head is carried upward by the tectonic velocity. Figure 11A shows one such small channel as it has begun to grow, giving the interfluve a wishbone morphology. With time the channel head reaches the main divide (fig. 11B and C) thereby forming a new first-order transverse river. This process is common and in the models shows no sign of

stabilizing (note next interfluve split starting in fig. 11C), but drainage density does not increase with time as drainage capture is also common and tends to keep the density of transverse rivers near constant.

This behavior leads to the conclusion that steadiness of topography is strongly scale dependent in the presence of horizontal motion. At the largest scale, the main divide will achieve a steady elevation and position relative to its baselevel boundaries, but at small scales, topographic features will be unable to migrate laterally to counter the tectonic displacement. They will therefore be laterally transported rather than remain in a fixed position. It is not clear what the scale threshold is for steady state of specific features, but the numerical models suggest that no features are steady, other than the main divide and the average cross-sectional form of the range.

## CONCLUSIONS

Theoretical considerations, numerical model results, and observations from three active orogens all indicate that the macrogeomorphology of mountain belts is strongly dependent upon $R$, the ratio of horizontal advection velocity to uplift velocity, $D$, the Peclet number representing the processes that wear down drainage divides, and $N_e$, a fluvial erosion number. In an orogenic system in which all mass is added by underplating, $R$ equals 0, and the time to steady state scales linearly and is expressed efficiently in terms of $D$ and $N_e$. For mountain belts with widths of 50 to 200 km, uplift rates of .1 to 1 mm/yr, and $N_e$ and $D$ values of about 1, times to steady state would range from about 1 to 50 my, with the longer times applicable to the lower uplift rates. If a significant fraction of the crustal mass is added to the orogen by frontal accretion, there will be a horizontal component to the surface velocity that gives rise to a migration of the main divide in the direction of this tectonic velocity. Steady state is reached when erosion processes acting on the divide drive it in the opposite direction at the horizontal tectonic velocity. Insofar as these erosion processes depend more on slope than on channelized water discharge, the motion of the main divide and its final, steady state position depend on the efficiency of diffusion and consequently the time to steady state is 5 to 10 times longer than for non-advective orogens.

The active orogens of Taiwan, the southern Alps of New Zealand, and the Olympic Mountains of Washington all show significant asymmetry in their across-strike topography such that in each case the retrowedge is steeper and shorter than the matching prowedge. While this might be caused by asymmetrical precipitation in the Olympics, the same cannot be said for the Southern Alps because the climatic asymmetry is opposite to the tectonic. In spite of this competition, the Southern Alps show the largest asymmetry of the three examples, with the polarity of the topography clearly supporting the tectonic motion as the dominant mechanism.

In addition to the gross asymmetry arising from horizontal advection in orogens, both field and model topographies show characteristic interfluve forms. On the side of the range facing the subducting plate, interfluves are commonly linear, or even slightly concave upward whereas on the opposite side interfluves are uniformly convex upward. In addition, we note that advective ridge migration during the approach to steady-state has the potential to control significantly orogen drainage. On the prowedge, longitudinal foreland rivers will be advected farther into the range with time, whereas on the retrowedge, advection moves material from channel heads toward the discharge point, so there is little opportunity for lateral river capture or advection. Drainage patterns in Taiwan and New Zealand reflect this control. Transverse rivers are uncommon on the prowedge in both cases, whereas on the retrowedge, the drainage pattern is characterized by parallel, transverse river catchments oriented perpendicular to the range trend.

ACKNOWLEDGMENTS

This research was supported by the National Science Foundation Grant EAR 95-26954. The manuscript was improved by helpful reviews by Mike Ellis, Peter van der Beek, and Peter Koons.

## References

Adams, J., 1980, Contemporary uplift and erosion of the Southern Alps, New Zealand: Geological Society of America Bulletin, Part II, v. 91, p. 1–114.

Ahnert, F., 1970, Functional relationships between denudation, relief, and uplift in large mid-latitude drainage basins: American Journal of Science, v. 268, p. 243–263.

Barry, R.G., 1981, Mountain Weather and Climate: London, Methuen, 313 p.

Batt, G.E., Brandon, M.T., Farley, K.A., and Roden-Tice, M., Tectonic synthesis of the Olympic Mountains segment of the Cascadia wedge using 2-D thermal and kinematic modeling of isotopic ages: Journal of Geophysical Research, in press.

Batt, G.E., and Braun, J., 1997, On the thermo-mechanical evolution of compressional orogens: Geophysical Journal, International, v. 128, p. 364–382.

Batt, G.E., Kohn, B.P., Braun, J., McDougall, I., and Ireland, T.R., 1999, New insight into the dynamic development of the Southern Alps, New Zealand, from detailed thermochronological investigation of the Mataketake Range pegmatites, *in:* Ring, U., Brandon, M.T., Lister, G.S., and Willett, S.D., editors, Exhumation Processes: Normal Faulting, Ductile Flow and Erosion: Geological Society of London, Special Publication 154, p. 261–282.

Beaumont, C., Fullsack, P., and Hamilton, J., 1992, Erosional control of active compressional orogens, *in* McClay, K.R., editor, Thrust Tectonics: London, Chapman and Hall, p. 1–18.

Beaumont, C., Kamp, P.J.J., Hamilton, J., and Fullsack, P., 1996, The continental collision zone, South Island New Zealand; Comparison of geodynamic models and observations: Journal of Geophysical Research, v. 101, p. 3333–3359.

Beaumont, C., Kooi, H. and Willett, S. D., 2000, Progress in coupled tectonic - surface process models with applications to rifted margins and collisional orogens, *in:* Summerfield, M., editor, Geomorphology and Global Tectonics: Chichester, Wiley, p. 29–56.

Beavan, J., Moore, M., Pearson, C., Henderson, M, Parsons, B., Bourne, S., England, P., Walcott, D., Blick, G., Darby, D., and Hodgkinson, K., 1999, Crustal deformation during 1994–1998 due to oblique continental collision in the central Southern Alps, New Zealand, and implications for seismic potential of the Alpine fault: Journal of Geophysical Research, v. 104, p. 25,233–25,255.

Brandon, M.T., and Calderwood, A.R., 1990. High-pressure metamorphism and uplift of the Olympic subduction complex: Geology, v. 18, p. 1252–1255.

Brandon, M.T, Roden-Tice, M.K., and Garver, J.I., 1998, Late Cenozoic exhumation of the Cascadia accretionary wedge in the Olympic Mountains, NW Washington State: Geological Society of America Bulletin, v. 110, p. 985–1009.

Brandon, M.T., and Vance, J.A., 1992, New statistical methods for analysis of fission-track grain-age distributions with applications to detrital zircon ages from the Olympic subduction complex, Western Washington State: American Journal of Science, v. 292, p. 565–636.

Braun, J., and Sambridge, M., 1997, Modelling landscape evolution on geological time scales: a new method based on irregular spatial discretization: Basin Research, v. 9, p. 27–52.

Chen, H., 1984, Crustal uplift and subsidence in Taiwan: an account based on retriangulation results: Central Geologic Survey Special Publication 3, p. 127–149.

Cooper, A.F., and Norris, R.J., 1994, Anatomy, structural evolution, and slip rate of a plate-boundary thrust: The Alpine Fault at Gaunt Creek, Westland, New Zealand: Geological Society of America Bulletin, v. 106, p. 627–633.

Crespi, J. M., Chan, Y.-C., and Swaim, M. S., 1996, Synorogenic extension and exhumation of the Taiwan hinterland: Geology, v. 24, p. 247–250.

Davis, D., Suppe, J., and Dahlen, F.A., 1983, Mechanics of fold-and-thrust belts and accretionary wedges: Journal of Geophysical Research, v. 88, p. 1153–1172.

Deffontaines, B., Lee, J., Angelier, J., Carvalho, J., and Rudant, J.-P., 1994, New geomorphic data on the Taiwan orogen: a multidisciplinary approach: Journal of Geophysical Research, v. 99, p. 20243–20266.

Densmore, A.L., Ellis, M.A., and Anderson, R.S., 1999, Numerical experiments on the evolution of mountainous topography: Journal of Geophysical Research, v. 103, p. 15203–15219,

Ellis, M.A., Densmore, A.L., and Anderson, R.S., 1999, Development of mountainous topography in the Basin Ranges, USA: Basin Research, v. 11, p. 21–41.

England, P., and McKenzie, D., 1982, A thin viscous sheet model for continental deformation: Geophysical Journal of the Royal Astronomical Society, v. 70, p. 295–321.

England, P., and Molnar, P., 1990, Surface uplift, uplift of rocks and exhumation of rocks: Geology, v. 18, p. 1173–1177.

Flint, J.J., 1974, Stream gradient as a function of order, magnitude, and discharge: Water Resources Research, v. 10, p. 969–973.

Hovius, N., Stark, C.P., and Allen, P.A., 1997, Sediment flux from a mountain belt derived by landslide mapping: Geology, v. 25, p. 231–234.

Hovius, N., Stark, C.P., Chu, H.-T., and Lin, J.-C., 2000, Supply and removal of sediment in a landslide-dominated mountain belt: Central Range, Taiwan: Journal of Geology, v. 108, p. 73–89.

Hurtrez, J. E., Lucazeau, F., Lave, J., and Avouac, J. P., 1999, Investigations of the relationships between basin morphology, tectonic uplift, and denudation from study of an active fold belt in the Siwalik Hills, central Nepal: Journal of Geophysical Research, v. 104, p. 12,779–12,796.
Kamp, P.J.J., Green, P.F., and White, S. H., 1989, Fission track analysis reveals character of collisional tectonics in New Zealand: Tectonics, v. 8, p. 169–195.
Khazaradze, G., Quamar, A., and Dragert, H., 1999, Tectonic deformation in western Washington from continuous GPS measurements: Geophysical Research Letters, v. 26, p. 3153–3188.
Kooi, H., and Beaumont, C., 1996, Large-scale geomorphology: Classical concepts reconciled and integrated with contemporary ideas via a surface processes model: Journal of Geophysical Research, v. 102, p. 3361–3386.
Koons, P.O., 1989, The topographic evolution of collisional mountain belts: a numerical look at the Southern Alps, New Zealand: American Journal of Science, v. 289, p. 1041–1069.
——— 1995, Modeling the topographic evolution of collisional belts: Annual Reviews Earth and Planetary Science, v. 23, p. 375–408.
Li, Y.H., 1976, Denudation of Taiwan island since the Pliocene epoch: Geology, v. 4, p. 105–107.
Liu, C. C., 1995, Geodetic monitoring of mountain building in Taiwan: EOS, Transactions of the American Geophysical Union, v. **76**, p. F634.
Liu, C.-C., and Yu, S.-B., 1990, Vertical crustal movements in eastern Taiwan and their tectonic implications: Tectonophysics, v. 183, p. 111–119.
Liu, T.K., 1982, Tectonic implication of fission-track ages from the Central Range, Taiwan: Proceedings of the Geological Society of China, v. 6, p. 133–152.
——— Fission-track dating of the Hsuehshan Range: Thermal record due to arc-cintinent collision in Taiwan: Acta Geoligica Taiwanica, v. 26, p. 279–280.
Maritan, A., Rinaldo, A., Rigon, R., Giacometti, A., and Rodriguez-Iturbe, I., 1996, Scaling laws for river networks: Physics Review, v. 53, p. 1510–1515.
Moglen, G.E., and Bras, R.L., 1995, The effect of spatial heterogeneities on geomorphic expression in a model of basin evolution: Water Resources Research, v. 31, p. 2613–2623.
Molnar, P., Anderson, H.J., Audoine, E., Eberhart-Phillips, D., Gledhill, K.R., Klosko, E.R., McEvilly, T.V., Okaya, D., Savage, M.K., Stern, T. and Wu, F.T., 1999, Continuous deformation versus faulting through the continental lithosphere of New Zealand: Science, v. 286, p. 516–519.
Munuz, J.A., 1992, Evolution of a continental collision belt: ECORS-Pyrenees crustal balanced cross-section, *in:* McClay, K.R., editor, Thrust Tectonics: London, Chapman & Hall, p. 235–246.
Norris, R.J., Koons, P.O., and Cooper, A.F., 1990, The obliquely-convergent plate boundary in the South Island of New Zealand: Implications for ancient collision zones: Journal of Structural Geology, v. 12, p. 715–725.
Pazzaglia, F.J., and Brandon, M.T., 2001, A fluvial reconrd of long-term steady-state uplift and erosion across the Cascadia forearc high, western Washington State: American Journal of Science, v. 301, p.
Pfiffner, O.A., 1992, Alpine Orogeny, *in* Blundell, D., Freeman, R., and Mueller, S., editors, The European Geotraverse: Cambridge, Cambridge University Press, p. 180–189.
Platt, J.P., 1986, Dynamics of orogenic wedges and the uplift of high-pressure metamorphic rocks: Geological Society of America Bulletin, v. 97, p. 1037–1053.
Pysklywec, R. N., Beaumont, C., and Fullsack, P., 2000, Modeling the behaviour of the continental mantle lithosphere during plate convergence: Geology, v. 28, p. 655–658.
Rinaldo, A., and Rodriguez-Iturbe, I., 1998, Scaling in river networks, *in:* Garrison, S., editor, Scale dependence and scale invariance in hydrology: Cambridge, United Kingdom, Cambridge University Press, p. 61–87.
Rodriguez-Iturbe, I., Ijjasz-Vasquez, E., Bras, R. L., and Tarboton, D.G., 1992, Power law distributions of discharge mass and energy in river basins: Water Resources Research, v. 28, p. 1089–1093.
Schmid, S.M., Pfiffner, O.A., Frotzheim, N., Schoenborn, G., and Kissling, E., 1996, Geophysical-geological transect and tectonic evolution of the Swiss-Italian Alps: Tectonics, v. 15, p. 1036–1064.
Seidl, M.A., and Dietrich, W.E., 1992, The problem of channel erosion into bedrock: Catena Supplement, v. 23, p. 101–124.
Seno, T., Stein, S., and Gripp, A.E., 1993, A model for the motion of the Philippine Sea plate consistent with NUVEL-1 and geological data: Journal of Geophysical Research, v. 98, p. 17,941–17,948.
Sinclair, K., and Ball, R., 1996, A mechanism for global optimization of river networks from local erosion rules: Physical Reviews Letters, v. 76, p. 3360–3363.
Slingerland, R., Willett, S.D., and Hovius, N., Slope-area scaling as a test of fluvial bedrock erosion laws: Eos, Transactions of the American Geophysical Union, v. 79, p. F358, 1998.
Snyder, N., Whipple, K., Tucker, G., and Merritts, D., 2000, Landscape response to tectonic forcing: digital elevation model analysis of stream profiles in the Mendocino triple junction region, northern California: Geological Society of America Bulletin, v. 112, p. 1250–1263.
Suppe, John, 1981, Mechanics of mountain building and metamorphism in Taiwan: Memoir of the Geological Society of China, v. 4, p. 67–89.
——— 1984, Kinematics of arc-continent collision, flipping of subduction, and back arc spreading near Taiwan: Memoir of the Geological Society of China, v. 6, p. 21–24.
Tabor, R.W., and Cady, W.M., 1978, The structure of the Olympic Mountains, Washington- Analysis of a subduction zone: U.S. Geological Survey Professional Paper 1033, 38 p.
Tarboton, D.G., Bras, R.L., and Rodriguez-Iturbe, I., 1991, On the extraction of channel networks from digital elevation data: Hydrological Processes, v. 5, p. 81–100.
Tippett, J.M., and Hovius, N., 2000, Geodynamic processes in the Southern Alps, New Zealand, *in* Summerfield, M., editor, Geomorphology and Global Tectonics: Chichester, Wiley, p. 109–134.

Tippett, J.M., and Kamp, P.J.J., 1993, Fission track analysis of the late Cenozoic vertical kinematics of continental Pacific crust, South Island, New Zealand: Journal of Geophysical Research, v. 98, p. 16119–16148.
Tsao, S., 1993, Illite crystallinity and fission track ages along the east Central Cross-Island Highway of Taiwan: Acta Geologica Taiwanica, v. 30, p. 65–94.
Tucker, G.E., and Slingerland, R.L., 1997, Drainage basin responses to climate change: Water Resources Research, v. 33, p. 2031–2047.
Walcott, R.I., 1978, Present tectonics, and late Cenozoic evolution of New Zealand: Royal Astronomical Society Geophysical Journal, v. 52, p. 137–164.
Walcott. R.I., 1998, Modes of oblique compression; late Cenozoic tectonics of the South Island of New Zealand: Reviews of Geophysics, v. 36, p. 1–26.
Wellman, H.W., 1979, An uplift map for the South Island of New Zealand, and a model for uplift of the Southern Alps, *in:* Walcott, R.I., and Cresswell, M.M., editors, The Origin of the Southern Alps: Bulletin of the Geological Society of New Zealand, v. 18, p. 13–20.
Whipple, K.X., and Tucker, G.E., 1999, Dynamics of the stream-power river incision model: Implications for height limits of mountain ranges, landscape response timescales, and research needs: Journal of Geophysical Research, v. 104, p. 17661–17674.
Whitehouse, I.E., 1987, Geomorphology of a compressional plate boundary, Southern Alps, New Zealand, *in* Gardiner, V., editor, International Geomorphology 1986, part I: New York, Wiley, p. 897–924.
Willemin, J.H., and Kneufer, P.L.K., 1994, Kinematics of arc-continent collision in the eastern Central Range of Taiwan inferred from geomorphic analysis: Journal of Geophysical Research, v. 99, p. 20267–20280.
Willett, S.D., 1999, Orogeny and orography: the effects of erosion on the structure of mountain belts: Journal of Geophysical Research, v. 104, p. 28957–28981.
Willett, S.D., Beaumont, C., and Fullsack, P., 1993, Mechanical model for the tectonics of doubly vergent compressional orogens: Geology, v. 21, p. 371–374.
Willgoose, G.R., Bras, R.L., and Rodriguea-Iturbe, I., 1991, A physically based coupled network growth and hillslope evolution model, 1. Theory: Water Resources Research, v. 27, p. 1671–1684.
Yu, S.-B., Chen, H.-Y., and Kuo, L.-C., 1997, Velocity of GPS stations in the Taiwan area: Tectonophysics, v. 274, p. 41–59.